REVIEW ARTICLE

VOLCANICA

The utility of TerraSAR-X, TanDEM-X, and PAZ for studying volcanic activity: Successes, challenges, and future prospects

Federico Galetto*[α], Edna Dualeh[β], Francisco Delgado[γ], Matthew Pritchard[α], Michael Poland[δ], Susanna K. Ebmeier[ε], Tara Shreve[ζ], Juliet Biggs[β], Ian Hamling[η], Christelle Wauthier[θ], Judit Gonzalez-Santana[θ], Jean-Luc Froger[ι], and Mark Bemelmans[β]

[α] Earth and Atmospheric Sciences Department, Cornell University, Ithaca, NY, USA.
[β] School of Earth Sciences, University of Bristol, Bristol, UK.
[γ] Department of Geology, Universidad de Chile, Santiago, Chile.
[δ] U.S. Geological Survey, Cascades Volcano Observatory, Vancouver, WA, USA.
[ε] School of Earth and Environment, University of Leeds, Leeds, UK.
[ζ] Geophysical Institute, University of Alaska Fairbanks, Fairbanks, AK, USA.
[η] GNS Science, Lower Hutt, New Zealand.
[θ] Department of Geosciences, The Pennsylvania State University, State College, PA, USA.
[ι] Université de Lyon, UJM-Saint-Étienne, UCBL, ENSLyon, CNRS, LGL-TPE UMR5276, F-42023, Saint-Étienne, France.

Submitted: 2023-09-15 | Accepted: 2024-04-09 | Published: 2024-06-04

Editor: T. Pering | Typesetter: G. N. Fabbro

Abstract

TerraSAR-X (TSX), TanDEM-X (TDX), and PAZ Synthetic Aperture Radar data have been used at over 120 volcanoes to assess surface characteristics and change over time. We examine previous work, adding additional examples to understand where and when these data are most useful for volcanology. We focus on volcanoes as part of the Committee on Earth Observation Satellites (CEOS) Volcano Demonstrator Project. TSX/TDX/PAZ data provide a valuable means of detecting small surface changes from amplitude images and topographic changes from bistatic TSX/TDX data. For short temporal and perpendicular baselines, TDX/TSX/PAZ can also provide useful deformation data, even in presence of vegetation. No global background mission currently acquires TSX/TDX/PAZ data at volcanoes: 70 % of CEOS volcanoes have no repeat high spatial resolution data, limiting their suitability for studying pre-eruptive unrest. Coordinated targeting by SAR constellations of priority volcanoes would provide data and insights valuable for forecasting eruptions and associated hazards.

Keywords: Global volcano monitoring; TanDEM-X; TerraSAR-X; PAZ; Bistatic TSX/TDX data.

1 Introduction

Less than 40 % of the world's ~1400 potentially active subaerial volcanoes are monitored continuously by ground-based systems due to the expense associated with the installation and maintenance of monitoring infrastructure [e.g. Loughlin et al. 2015; National Academies of Sciences, Engineering & Medicine 2017; Whitehead and Bebbington 2021]. Satellite observations can help to fill some gaps in volcano monitoring, and different types of sensors spanning the electromagnetic spectrum have been used to track volcanic activity before, during, and after eruptions [e.g. Valade et al. 2019; Poland et al. 2020; Pritchard et al. 2022a]. For decades, volcanic surface change detection and mapping from satellites has relied primarily on imagery with spatial resolutions of order 10–30 m pixel^{-1} and repeat intervals of weeks to months [e.g. Landsat, SPOT, ERS-1/2, ENVISAT, Sentinel-1; Francis and De Silva 1989; Chorowicz et al. 1992; Flynn et al. 2001; Lu and Dzurisin 2014]. An exciting advance in satellite observations of volcanoes is the development of radar and optical datasets with spatial resolutions of 3 m pixel^{-1} or lower with repeat intervals of a week or less (e.g. Planet, WorldView, Pléiades, Radarsat-2, TerraSAR-X, COSMO-SkyMed, Capella, ICEYE) that have allowed investigations of critical, smaller-scale features and their changes over time [Richter et al. 2013; Eugenio et al. 2014; Aldeghi et al. 2019; Waythomas et al. 2020; Dai et al. 2022; Bemelmans et al. 2023]. For example, high spatial resolution Synthetic Aperture Radar (SAR) images from RADARSAT-2 and TerraSAR-X satellites showed changes before an eruption at Merapi, Indonesia and were used along with other data to inform evacuation orders that saved thousands of lives in 2010 [Pallister et al. 2013].

One of the longest-lived high spatial resolution SAR constellations includes X-band (3.1 cm) satellites TerraSAR-X (TSX; launched 2007) and TanDEM-X (TDX, launched 2010), of the German Aerospace Center (DLR), and the Spanish satellite PAZ (launched 2018), which all utilize the same orbital characteristics and have very similar acquisition capabilities. To date, more than 80 volcanoes and geothermal areas have been studied with TSX and TDX data, and a small number with PAZ (Figure 1; Supplementary Material 1 Table S1). The TSX/TDX/PAZ datasets have provided unique information about volcanoes because of their high spatial resolution all-weather SAR modes with a 4-, 7-, and 11-day repeat interval, as well as the bistatic topographic mapping capability of the Co-registered Single-look Slant-range Complex images (CoSSCs) [Kubanek et al. 2018; 2021]. Examples of unique signals at volcanoes discovered with TSX/TDX that could not be clearly seen with lower spatial resolution SAR sensors (such as Sentinel-1) include: spotlight mode interferograms showing deformation in a region of ~250 m in diameter at Volcán Colima, Mexico [Salzer et al. 2014; 2017], topographic change from a small eruption at Volcán Hudson, Chile [Pritchard et al.

* fg253@cornell.edu

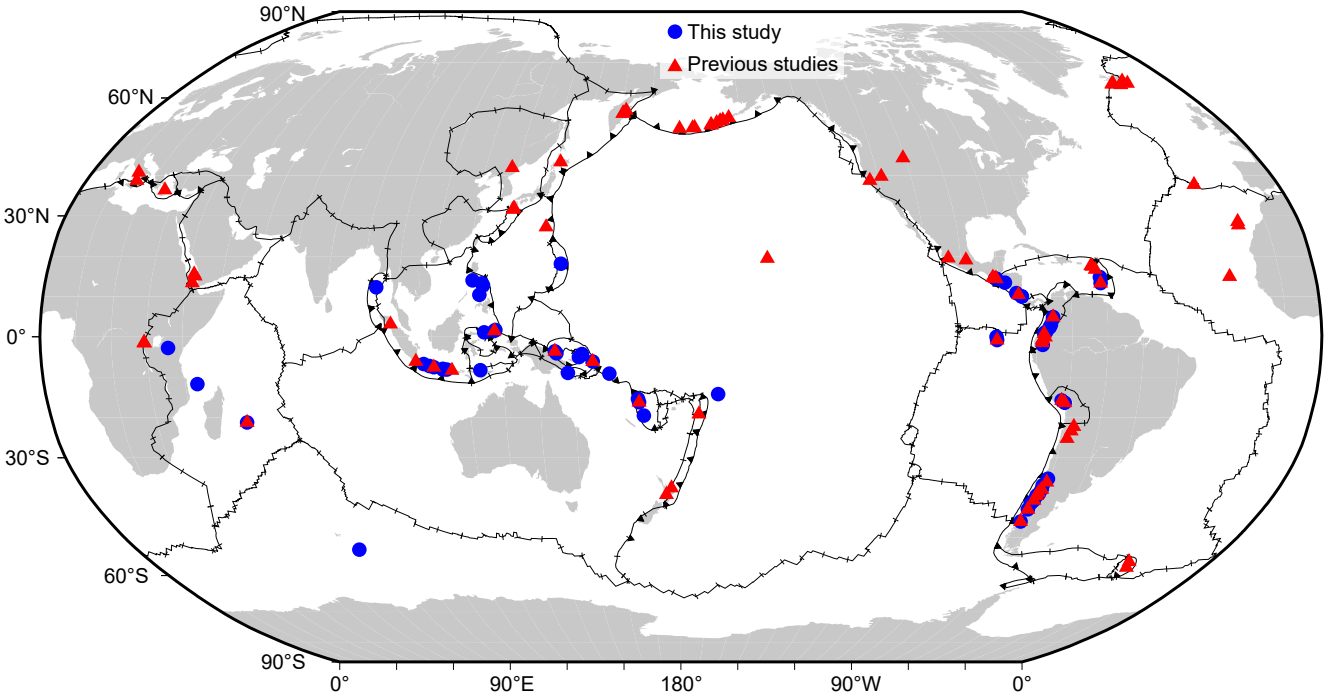

Figure 1: Volcanoes analyzed with TSX/TDX/PAZ data in previous studies (red triangles, see Supplementary Material 1 Table S1) and this work (blue circles, see Table 1 for volcano names and types of data used). Boundaries of tectonic plates shown by black lines [from Bird 2003].

2018], and amplitude changes of repeated lava dome formation and destruction within the inner crater at Popocatépetl, Mexico [Valade et al. 2023].

Because TSX/TDX/PAZ and other high-spatial-resolution satellite imagery is usually restricted to commercial users or scientific investigators with approved proposals, its use at volcanoes has been limited, and so the value and limits of these datasets for global volcano science and hazards assessment have not been fully explored. Further, the performance of SAR observations depends on the type of ground cover and the radar wavelength, among other parameters [e.g. Pritchard et al. 2018], and the TSX/TDX/PAZ data have shown different levels of success (and failure) at different volcanoes and geothermal areas of the world (see Supplementary Material 1 Table S1). For instance, several studies have established that X-band InSAR is more challenging in vegetated areas than longer radar wavelengths [e.g. Pritchard et al. 2018; Sica et al. 2021]. Our objective is to review and augment previous TSX/TDX/PAZ studies with new analysis of those data from volcanoes that span a range of environments to answer the following questions: How many volcanoes have surface or topographic change detectable with TSX/TDX/PAZ versus insufficient data quality (in terms of spatial or temporal sampling) to detect such changes? Does the utility of TSX/TDX/PAZ vary depending on the observation mode, type of volcano, or environmental conditions? Currently, we do not yet know how many volcanoes have surface or topographic changes that can be detected using high-resolution satellite imagery (<3 m pixel^{-1}). Based on the limited literature available, dozens of volcanoes annually might exhibit changes in the high-resolution data that might be missed using other techniques [e.g. Bemelmans et al. 2023]. For example, in a reconnaissance study, Pritchard et al. [2018] noted that >35 % of the potentially active volcanoes in Latin America had topographic changes resolvable from space.

Access to TSX/TDX/PAZ data is provided through several avenues, including individual research projects directly with DLR, the Committee on Earth Observation Satellites (CEOS) Volcano Demonstrator project, which aimed to monitor all ~720 subaerial Holocene volcanoes in Africa, Latin America, and Southeast Asia [Delgado et al. 2019b; Sansosti et al. 2019; Pritchard et al. 2022b]*, the NASA Commercial Smallsat Data Acquisition program, and the Geohazards Supersites and Natural Laboratories initiative from the Group on Earth Observations [Salvi 2016]. In addition to using archived data, as part of the CEOS Volcano Demonstrator we requested TSX/TDX/PAZ tasking at 57 volcanoes that were either not receiving sufficient background data acquisition or needed more frequent data collection because of increased volcanic activity. The end goal of the CEOS Volcano Demonstrator is to develop an integrated, international, global remote sensing geohazards monitoring effort for disaster risk management, following the 2012 Santorini report [Bally 2013]. The five-year CEOS Volcano Demonstrator (spanning 2019–2023) focused on about 50 % of Holocene volcanoes across three geographic regions to demonstrate the utility of the satellite observations for end users (i.e. the volcano observatories that are governmentally responsible for volcano monitoring) and to research ways in which the observation strategy can be optimized to exploit the unique advantages of each type of sensor. The CEOS Volcano Demonstrator builds on the success of a smaller pi-

*https://ceos.org/ourwork/workinggroups/disasters/volcanoes/

Table 1: Volcanoes analyzed in this work (listed by country).

GVP id[a]	Volcano name	Country	Asc.[b]	Desc.[c]	Mode[d]
342090	Fuego	Guatemala	54	63	SL
342110	Pacaya	Guatemala	90	82	SL (T)
			166	6	CoSSC (T)
343100	San Miguel	El Salvador	n/a	97	SM (T)
345020	Rincon de la Vieja	Costa Rica	14	21	SL (T)
345060	Irazu	Costa Rica	33	n/a	SL (T)
345070	Turrialba	Costa Rica	14	n/a	SL (T)
360120	Pelee	Martinique	104	20	SL (T)
360150	La Soufrière St. Vincent	West Indies	85	23	SL (T)
351020	Nevado del Ruiz	Colombia	72	n/a	SM (T)
351040	Cerro Machin	Colombia	5	13	SM (T)
351050	Nevado del Huila	Colombia	11	n/a	SM (T)
351060	Purace	Colombia	44	142	SL (T)
351080	Galeras	Colombia	3		SM (T)
351100	Cumbal	Colombia	10	12	SM (T)
351110	Chiles	Colombia/Ecuador	10	n/a	SM (T)
353020	Wolf	Ecuador (Galápagos)	74	6	SM (T)
353050	Sierra Negra	Ecuador (Galápagos)	74	n/a	SM (T)
			74	n/a	CoSSC (T)
352090	Sangay	Ecuador	119	142	SM (T)
354006	Sabancaya	Perú	134	n/a	CoSSC (T)
354020	Ubinas	Perú	134	96	SM (T)
357040	Planchon-Peteroa	Chile/Argentina	104	n/a	SL (T)
357070	Chillan, Nevados de	Chile	8	n/a	SM (T)
			n/a	10	SL (T)
357090	Copahue	Chile	8	7	SM (T)
357111	Sollipulli	Chile	28	111	SM (T)
357120	Villarrica	Chile	104	111	SM (T)
357150	Puyehue-Cordon Caulle	Chile	104; 13	111; 35	CoSSC (T)
			9	7	SM (T)
358020	Calbuco	Chile	13	n/a	CoSSC (T)
			6	8	SM (T)
358041	Chaiten	Chile	13	n/a	SM (T)
358057	Cerro Hudson	Chile	13	4	SM (T)
			89	n/a	CoSSC (T)
222120	Ol Doinyo Lengai	Tanzania	n/a	122	SL (T)
233010	Karthala	Comoros	114	152	SM (T)
233020	Piton de la Fournaise	France (La Réunion Is)	121	7	SL (T/P)
234010	Heard	Australia	n/a	135	CoSSC (T)
260010	Barren Island	India	n/a	150	HS (T)
263090	Tangkuban Parahu	Indonesia	96	n/a	SM (T)
263180	Slamet	Indonesia	96	134	SL (T)
263250	Merapi	Indonesia	n/a	58; 111	SL (T/P)
263300	Semeru	Indonesia	111	149	SL (T)
263310	Tengger caldera	Indonesia	20	n/a	SL (T)

[a] GVP id is the identification number of each volcano in the Smithsonian Global Volcanism Program database [Global Volcanism Program 2022], which contains information about each volcano and its activity.

[b] Asc. = ascending relative orbit number analyzed in this work

[c] Desc. = descending relative orbit number analyzed in this work.

[d] Mode is the product analyzed in this work (SM = Stripmap; SL = Spotlight; HS = High Resolution Spotlight; CoSSC = bistatic TDX/TSX pairs). T = TDX/TSX data; P = PAZ data. Other technical information about these data is available at https://eoweb.dlr.de/guestegp/main#mainWindowtabExplore

Table 1: Volcanoes analyzed in this work (listed by country).

GVP id	Volcano name	Country	Asc.	Desc.	Mode
263340	Raung	Indonesia	35	n/a	SM (T)
			111	149	CoSSC (T)
264230	Lewotolok	Indonesia	65	12	HS (T)
266030	Soputan	Indonesia	157	n/a	SM (T)
268030	Ibu	Indonesia	82; 80; 156	27	CoSSC (T)
268010	Dukono	Indonesia	5	103	SL (T)
272020	Kanlaon	Philippines	157	164	SL (T)
273010	Bulusan	Philippines	34	24	SL (T)
273030	Mayon	Philippines	28	34	SM (T)
273070	Taal	Philippines	5; 14	n/a	SM (T)
			n/a	48; 94	SL (T)
284170	Pagan	Mariana Islands (CNMI)	80	72	SL (T)
			n/a	n/a	
251002	Kadovar	Papua New Guinea	36	23	SL (T)
251020	Manam	Papua New Guinea	43	12	SL (T)
252120	Ulawun	Papua New Guinea	35; 79	58	SL (T)
			n/a	3	SM (T)
252140	Rabaul	Papua New Guinea	3	n/a	SM (T)
			n/a	26	HS (T)
253010	Lamington	Papua New Guinea	42	16	SL (T)
255020	Bagana	Papua New Guinea	21	16	SL (T)
255070	Savo	Solomons Is.	109	56	SL (T)
257030	Ambae	Vanuatu	124	10	SL (T)
257040	Ambrym	Vanuatu	48; 21	86; 17	SL (T)
257100	Yasur	Vanuatu	48	10	SL (T)
244020	Tau (Tutuila)	American Samoa	32; 123	9; 85	SL (T)

lot project that focused on Latin America and that was active during 2013–2017 [Pritchard et al. 2018].

2 Methodology

Here and in previous works, the TSX/TDX/PAZ data have been used to make three different categories of measurements at volcanoes that each involve different approaches and data products [e.g. Pritchard and Yun 2018]:

1. Ground deformation and coherence maps derived from Interferometric Synthetic Aperture Radar (InSAR) are used to quantify ground deformation [e.g. Wang et al. 2018] and surface-coherence change caused by volcanic deposits (tephra, lava, lahars, domes, pyroclastic density currents) or mass removal (flank movements, formation of explosion craters and calderas) [Matthews et al. 2003; Dualeh et al. 2021; Walter 2023]. Both differential InSAR and measurement of coherence using TSX/TDX/PAZ involves combining Single look Slant range Complex (SSC) images acquired on different dates. To measure ground deformation, orbital information provided by the space agencies and Digital Elevation Models (DEMs) are used to remove orbital and topographic effects. InSAR ground deformation measurements can be affected by changes in atmospheric water vapor that can be estimated using weather models; however, such models typically do not resolve features <10 km in scale, which are the focus of the high-spatial-resolution data studied here [Bemelmans et al. 2023]. Further, comparing interferograms with and without weather model corrections did not show significant differences at Masaya volcano, Nicaragua [Stephens et al. 2020] and San Miguel volcano, El Salvador (Supplementary Figures page 136; Supplementary Figures file available in the data repository*). Lack of any substantive difference is likely due to a combination of topographic effects and a low density of measurements underpinning weather models in Central America. Other studies have shown varying degrees of success using weather models to correct changes in atmospheric water vapor [Parker et al. 2015; Delgado et al. 2017; Delgado and Grandin 2021]. Thus, we do not use atmospheric corrections in this study, consistent with most of the studies cited herein. Analyzing a time series of SAR images using a multi-temporal approach (e.g. persistent scatters or small baselines) helps to reduce errors and to detect small deformation [Hooper et al. 2012], but the main limitation with TSX data is that for most volcanoes there are few available TSX/TDX scenes and so multitemporal approaches are not applicable.

2. Surface-change maps using SAR backscatter or amplitude data acquired over time at the same volcano [National Academies of Sciences, Engineering & Medicine 2017]. By comparing SAR amplitude data over time it is possible to identify and track surface change connected to volcanic activity, such as new or growing lava flows (or other volcanic

*https://osf.io/35xud/

flows like pyroclastic density currents and lahars), domes and lava lakes, and changes at volcanic vents due to explosions, caldera collapse, or the growth of a new cone [e.g. Dualeh et al. 2021; Barrière et al. 2022; Dualeh et al. 2023; Smittarello et al. 2023; Valade et al. 2023]. We analyze SSC images in native radar coordinates to create time series of amplitude changes (see Section 3.2 and Supplementary Figures). In addition, if deformation produces geometric distortions without significantly affecting the SAR image reflectivity, displacements can be calculated directly from the amplitudes of SAR images acquired over time through pixel-offset tracking [Casu et al. 2011; Pinel et al. 2014]. This technique measures deformation in the along- and across-track directions using normalized cross correlation of windows of pixels and has a lower sensitivity to deformation than InSAR, but does not suffer from phase aliasing in zones of large strain [Casu et al. 2011; Shreve and Delgado 2023].

3. Topographic change using TanDEM-X bistatic interferometry can quantify height and volume variations associated with volcanic eruptions [National Academies of Sciences, Engineering & Medicine 2017; Kubanek et al. 2021]. Bistatic pairs consist of one TSX and one TDX SAR image of the same area acquired at the same time that can be used to compute a DEM and to calculate the topographic change with respect to a reference DEM (see Kubanek et al. [2015a, 2021] for further details on this methodology). Any changes in elevation that occurred between the times of acquisition of the reference DEM and the bistatic pair due to volcanic activity can be therefore mapped at the spatial resolution of the DEM (or of the bistatic TDX/TSX pair if it has an equal or lower resolution than that of the DEM). Topographic changes can be caused by lava flows and domes, pyroclastic density currents, large tephra deposits, growth or destruction of a cone, and large-scale flank or caldera collapses, each of which has a different characteristic spatial and temporal scale.

We have compiled previously published results that used TSX/TDX/PAZ data from more than 80 volcanoes and geothermal areas (Figure 1) and noted which of the three approaches above were used (see Supplemental Table 1). We further analyzed 57 volcanoes throughout the CEOS Volcano Demonstrator and other regions that had not been previously studied with available TSX/TDX/PAZ SAR data (Table 1; Figure 1). Volcanoes were selected to demonstrate TSX/TDX/PAZ SAR data in different environments (desert, ice-clad, vegetated) and different types of eruptions (explosive, effusive) or without eruption to assess the overall data quality.

For data analysis, we use both the InSAR Scientific Computing Environment (ISCE) software [Rosen et al. 2015] and Gamma software [Werner et al. 2000]. We used the following products: (1) StripMap (SM) data with a spatial resolution of ~3 × 3 m pixel^{-1} in azimuth and range; (2) High Resolution SpotLight data (HS) with a spatial resolution up to 1 m pixel^{-1} in azimuth and up to 1.5 in range; (3) SpotLight (SL) data with a spatial resolution up to 2 m pixel^{-1} in azimuth and up to 1.5 in range; and (4) bistatic TDX/TSX pairs, which consist of two SAR images acquired at approximately the same time, with a spatial resolution that depends on the mode of acquisition (SM, SL, HS). A trade-off exists between spatial resolution and the area covered by the data, with higher pixel resolution (HS and SL) data that have a smaller footprint, covering a smaller area, than those with a lower pixel resolution (SM).

For all these types of measurements, high-resolution DEMs are necessary to correct topographic distortions and accurately georeference products without significant loss of resolution [e.g. Bemelmans et al. 2023; Grémion et al. 2023]. However, in most of the cases we did not have access to high-resolution DEM; therefore, we used open source 30-m resolution DEMs: the NASA Shuttle Radar Topography Mission (SRTM) DEM, acquired in 2000, and the Copernicus DEM [Farr et al. 2007; European Space Agency]. The Copernicus DEM comes from the interpolation of multiple TDX/TSX data acquired from 2011 to 2015 and therefore does not have a specific date of acquisition. For this reason, we preferred to use the SRTM DEM, limiting the use of the Copernicus DEM only to cases where it was necessary to use an updated DEM. When available, we used higher spatial resolution DEMs, such as WorldDEM, acquired in 2012, and Pléiades [Bernard et al. 2012; Riegler et al. 2015; Wessel 2018], as noted in the captions, to achieve the highest spatial resolution for the derived products (e.g. ground deformation maps and topographic change maps). In some instances, when high-resolution DEMs were not available, and we needed to show features that would be obscured by the 30-m DEMs resolution, we interpolated the 30-m DEMs to the full resolution of the TSX/TDX/PAZ data [see figure captions; Arnold et al. 2017].

3 Results

For most of the volcanoes and geothermal areas that we analyzed (Table 1; Figure 1), we created a short report on examples of data quality for the different observation modes (Supplementary Figures file and all the reports are available in the data repository*). These reports may be useful to researchers who want to evaluate data quality at a given volcano before utilizing TSX/TDX/PAZ data. Below, we summarize key results on data quality for different volcanoes from the three data analysis categories: InSAR and coherence maps, surface change from amplitude data, and topographic changes from bistatic TSX/TDX pairs.

3.1 InSAR and coherence maps

Several studies have established that X-band InSAR is more challenging in vegetated areas than longer radar wavelengths [e.g. Pritchard et al. 2018; Sica et al. 2021]. As expected, we find that coherence degrades with the increase of the temporal baseline of the interferogram, especially in areas with overall low coherence, such as vegetated areas. However, useful data can be acquired even at heavily vegetated volcanoes when the time period is short (days to a few weeks) and the orbital separation, known as the perpendicular baseline, is small (<100 m). This is shown in Figure 2, where good coherence is maintained in the vegetated area of San Miguel volcano (El Salvador) when using small temporal and perpendicular baselines, but the coherent area significantly decreases for larger baselines. Few centimeters of deformation occurred at San

*https://osf.io/35xud/

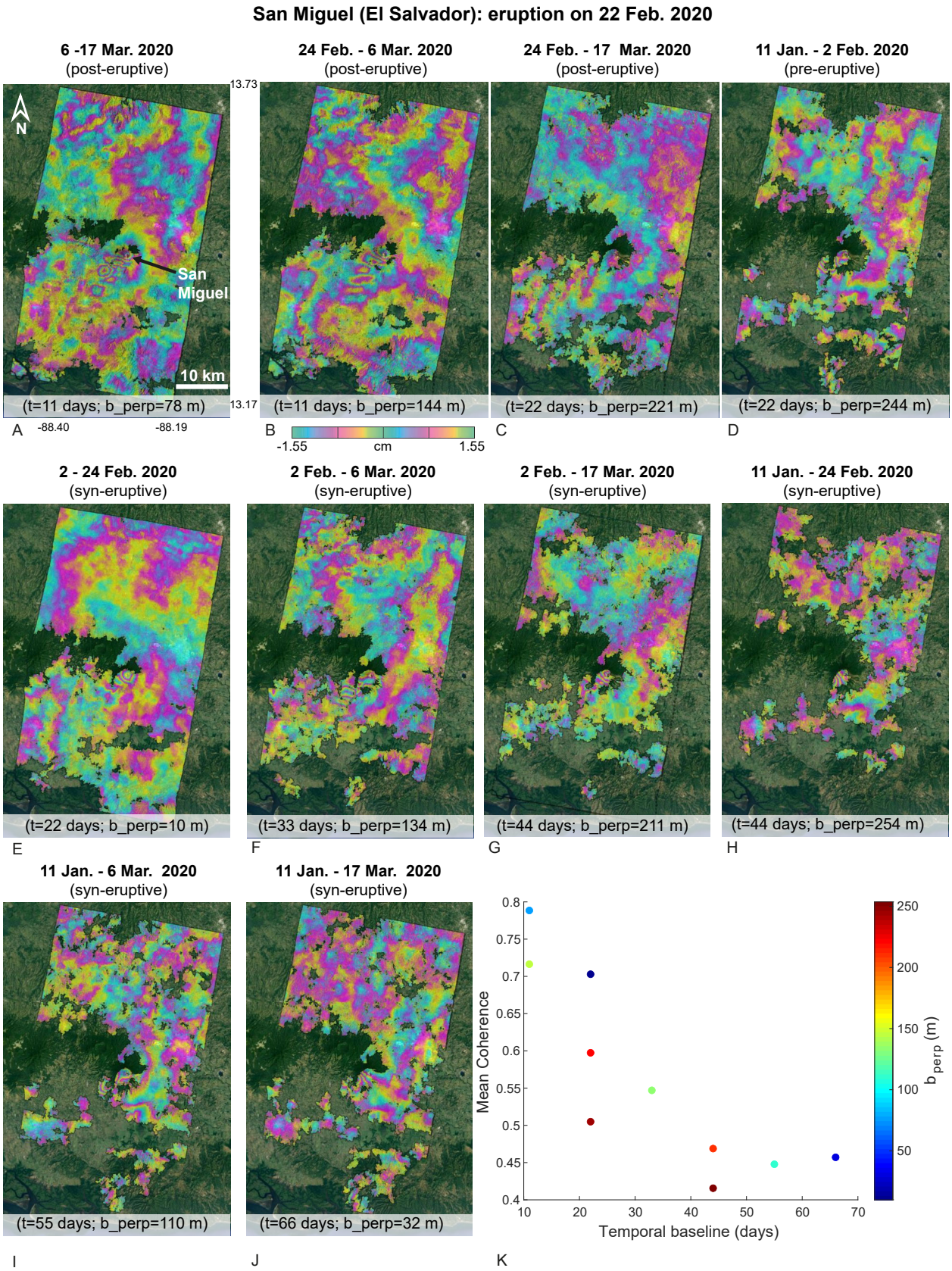

Figure 2: Stripmap descending data interferograms spanning different time intervals at San Miguel volcano, El Salvador (Table 1). A NASA-SRTM 30 m DEM was used to remove the topographic effects on interferograms. [A–J] Interferometric Synthetic Aperture Radar (InSAR) data obtained using different temporal resolution and different perpendicular baselines. [K] Change in the mean coherence of each interferogram as a function of the temporal (t) and perpendicular baseline (b_perp).

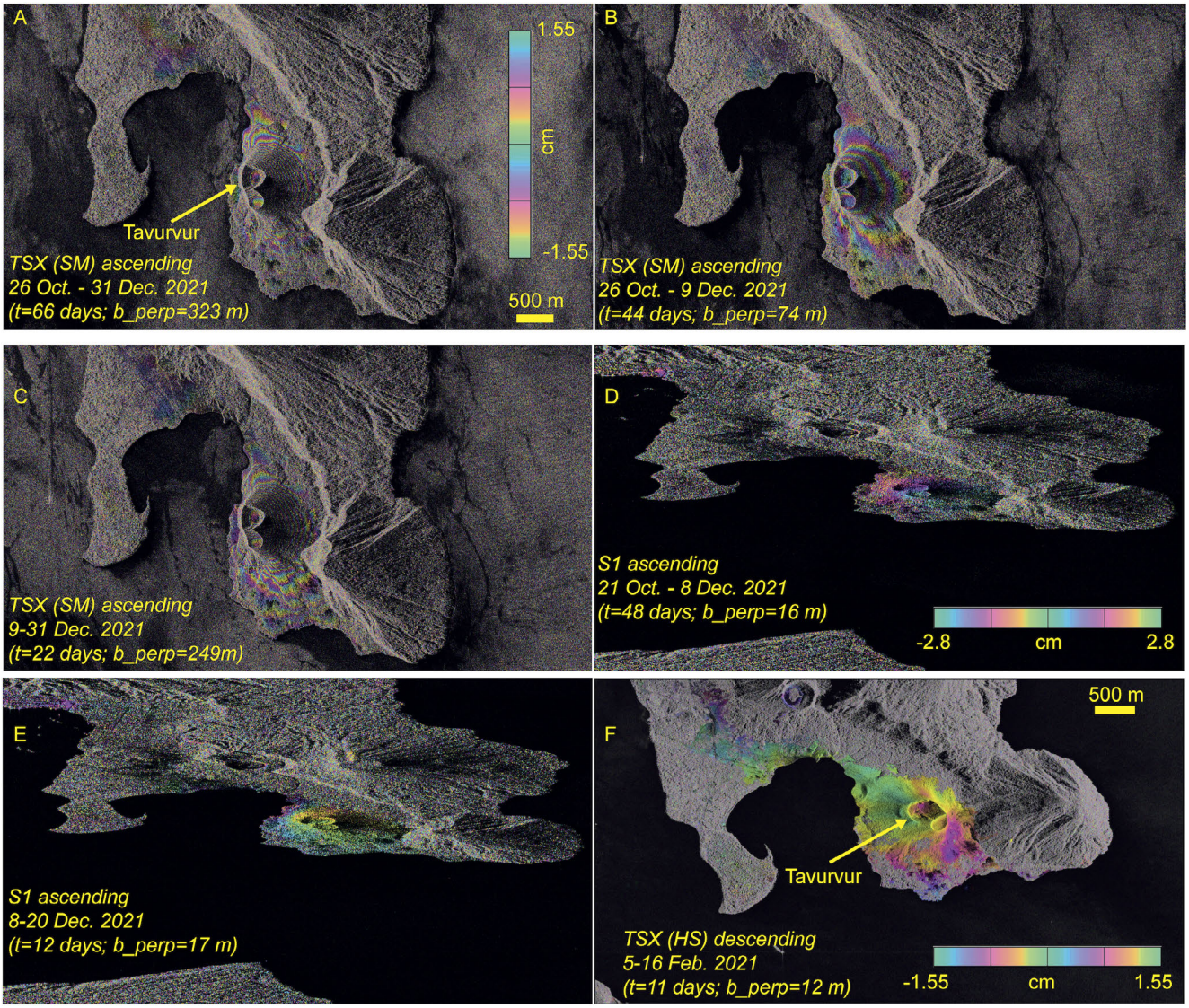

Figure 3: Comparison between different wrapped InSAR data at Tavurvur volcano (Table 1), inside the Rabaul caldera, Papua New Guinea. [A–C] Stripmap data (interferogram in panel a covers the entire time-period of the interferograms reported in panels B and C. [D–E] Sentinel-1 data covering a similar time span of interferograms in panels b and c, respectively. [F] High Resolution (HS) data. SRTM topography [Farr et al. 2007] was used to remove the topographic effects on all interferograms. The SRTM data were interpolated to 3 m pixel^{-1} for panel A–C, 2 × 14 m pixel^{-1} for D–E, and 1 m pixel^{-1} for F, in order to process all interferograms at full resolution. All images are in radar coordinates and have been flipped (horizontally and/or vertically) in order to be consistent with each other.

Miguel during the pre- and syn-eruptive period of the eruption that occurred on 22 February 2020 (Figure 2D, E, G, H, J). Signals associated with the image acquired on 6 March are likely atmospheric contributions (as evident by comparing Figure 2B–C), although we were not able to completely remove these signals with the ERA-5 atmospheric model implemented in MintPy with the PyAPS software [Supplementary Figures pages 136; Jolivet et al. 2014; Yunjun et al. 2019]. Similar results related to coherence have been obtained with HS mode data at Lewotolok (Indonesia), where small temporal and perpendicular baselines provide better coherence than interferograms from large temporal and perpendicular baselines, allowing detection of ground displacements in an area characterized by steep topography (Supplementary Figures pages 52–55).

The presence of less-vegetated areas along the flanks of a volcano can enhance the use of TSX/TDX/PAZ data for volcano monitoring, as shown at Soputan volcano in Indonesia (in Supplementary Figures pages 156–158). Here, although the SM coherence of the whole image is low due to the vegetation, the flank of the volcano has good coherence even for temporal separations >1 yr^{-1} because of low vegetation cover in that region. This allows for assessment of surface deformation at Soputan at a high spatial resolution, supporting the use of these data for volcano monitoring. Other equatorial and tropical volcanoes show some areas with high coherence,

usually in areas of low vegetation cover, that allow the use of these high resolution data (e.g. Ulawun, Barren Island, Bagana, Cumbal, Turrialba, Tengger Caldera, and Lewotolok), while others are completely incoherent even with only 11 days of temporal baseline (e.g. Tangkuban Parahu and Cerro Machin and other volcanoes reported in the Supplementary Figures), which is the shortest temporal resolution when no PAZ data are available to complement the TSX/TDX data. SM data of Rabaul caldera, characterized by an overall very low coherence (Supplementary Figures pages 104–109), show that some coherence is maintained within the caldera area and in particular near Tavurvur volcano (Figure 3A–C and Supplementary Figures pages 105–109). Here, the SM data processed at full resolution (about 3 m pixel^{-1} spatial resolution in range and azimuth) reveal ground deformation associated with the Tavurvur cone (Figure 3A–C), which would be more difficult to detect using InSAR data with lower spatial resolution, like Sentinel-1 (about 2 m pixel^{-1} by 14 m pixel^{-1} in the range and azimuth, respectively; Figure 3D–E). Tavurvur volcano is also covered by HS data (1 m spatial resolution; Figure 3F) that can be used together with SM data to monitor Rabaul caldera due to the excellent coherence of the HS data in the area of Tavurvur volcano. In addition, Figure 3A–C, F show the importance of having both the ascending and the descending orbit data to properly study all the flanks of this volcano. Thus, X-band data, like those acquired by TSX/TDX satellites, are very helpful to monitor this small (0.1 km^2 summit craters and 1 km^2 volcanic edifice) but very active volcano [see Bernard and Bouvet de Maisonneuve 2020 for recent eruption history of Tavurvur], whose deformation would be more difficult to detect with longer wavelengths (Figure 3).

In Figure 4 we report further examples of volcanoes where TSX data are able to successfully detect ground displacements connected with the volcanic activity, such as co-eruptive subsidence of the caldera floor of Wolf volcano (Galápagos, Ecuador; Figure 4A), inter-eruptive deformation of the volcanic edifice of Ambrym volcano (Vanuatu; Figure 4B–E), and co-eruptive deformation at Piton de la Fournaise (La Réunion Island; Figure 4F–G). These deformation signals are confirmed by other SAR satellites [Shreve et al. 2023; Xu et al. 2023], supporting the possibility of integrating TSX/TDX data with other SAR data to improve the temporal coverage for a volcano. In the Supplemental Figures, we show other examples of several volcanoes with InSAR-detected ground deformation from TSX/TDX data that were not previously published. At Ulawun, Papua New Guinea (Supplementary Figures pages 200–203), we observe some post-2019 eruption signals, which are significant because previous InSAR studies using ALOS-2 data were not able to resolve any signal at Ulawun prior to the 2019 eruption [McKee et al. 2021b].

The combination of TSX and PAZ data to generate TSX–PAZ interferograms can further reduce the temporal baselines of the interferograms (4- and 7-day spans). In Figure 5A–C, we show an example TSX–PAZ interferogram (SL mode) for Merapi indicating localized flank deformation characterized by high-rates of motion that occurred during 3–7 December 2020, a few weeks prior to the onset of eruptive activity in January 2021. These data were communicated to local volcanologists who were monitoring the volcanic unrest at the time of the crisis and aided their response to the activity [Poland and Zebker 2022]. This example emphasizes the potential of the TSX/TDX/PAZ constellation to monitor volcanic unrest, especially when high rates of surface displacement make short-timespan interferometry necessary. In Figure 5d we show for comparison a Sentinel-1 interferogram of the same area. The spatial resolution of Sentinel-1 data does not allow detection of the deformation that occurred on the northern flank (Figure 5). In addition, the minimum temporal resolution of Sentinel-1 is 12 days, which does not allow a full appreciation of the very rapid displacements. For this reason, the possibility of obtaining high-resolution interferograms with a temporal baseline of 4 days represents a powerful tool to monitor high-rate volcano deformation in focused areas during unrest.

Previously published articles (Supplementary Material 1 Table S1) reported other cases in which InSAR TSX/TDX SM data provided useful information despite difficult environmental conditions, such as the VEI ≥ 4 eruptions at Chaiten (2008–2009) and Cordon Caulle (2011–2012) [Delgado et al. 2019a; 2022]. Both volcanoes are surrounded by dense temperate rainforest, and the eruptions occurred during the austral winter. These two factors led to high interferometric coherence loss, made even worse by the ash deposition during the Plinian phases of these events. Despite these conditions, useful information was still obtained from these data, such as an overall lack of deformation observed during the effusive phase of Chaiten eruption, and a significant deformation observed during the onset of the Cordon Caulle eruption [Delgado et al. 2019a; 2022]. Time series of deformation obtained with TSX data can be helpful also to reduce errors and to reveal volcanic unrest characterized by small deformation rates [e.g. MacQueen et al. 2020]; however, most of the analyzed volcanoes did not have enough data for time-series analysis.

3.2 SAR amplitude data

Here we report some examples of different surface changes connected to volcanic activity that can be detected from TSX/TDX data. Figure 6 shows the ability of the HS mode to detect the emplacement and growth of multiple lava flows within small craters, such as that of the Lewotolok volcano (area of ~0.7 km^2). These flows cannot be detected by open-access C-band SAR amplitude data, like Sentinel-1, which are characterized by lower spatial resolution (Supplementary Figure page 51), highlighting the importance of access to HS data during a volcanic eruption. Figure 6 also highlights the importance of having a time series for both ascending and descending satellite orbits to better detect surface change in areas of steep topography with significant radar layover and foreshortening distortions. A general advantage of SAR amplitude data is that they are not affected by atmospheric clouds, volcanic gas (or gas + ash), or time of day; therefore, lava flow/dome growth can be tracked in any condition. In contrast, optical and thermal data, which are not affected by geometric distortions because of their generally more vertical look angles, are blind in the presence of clouds and/or volcanic emissions and, as for optical data, at night. This is evident by comparing the HS data (Figure 6A–F) with the available cloud-free Sentinel-2

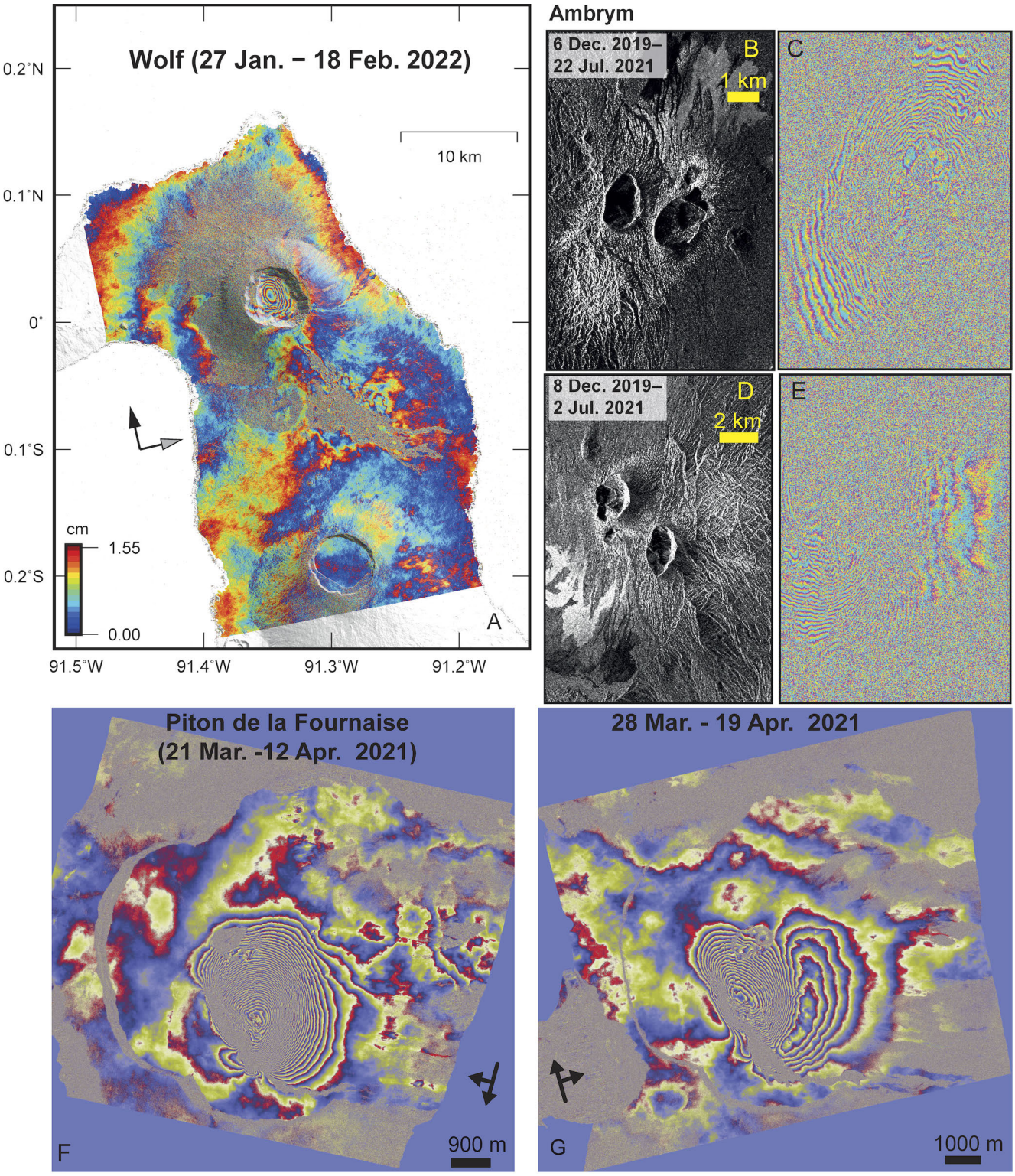

Figure 4: Examples of deforming volcanoes from TSX/TDX/PAZ interferograms. [A] Wrapped Line of Sight (LOS) displacements recorded by Stripmap data at Wolf volcano (Galápagos; Table 1). The 12-m resolution WorldDEM topography [Wessel 2018] was used to remove the topographic effects. [B, D] Amplitude data (B from the ascending orbit and D from the descending orbit) of Ambrym volcano (Vanuatu; Table 1) (SL mode) and [C, E] the associated wrapped LOS displacements [Shreve et al. 2023]. WorldDEM was again used to remove topographic effects. [F–G] Wrapped LOS displacements recorded by Spotlight PAZ data at Piton de la Fournaise (La Réunion Island; Table 1). A 5-m DEM produced by the French Geographic Institute (IGN) via lidar in 2008–2009 was used to remove topographic effects. Each fringe (full color cycle) represents 2π radians of phase change corresponding to 1.55 cm of range change in the LOS direction in panels C, E, F, G.

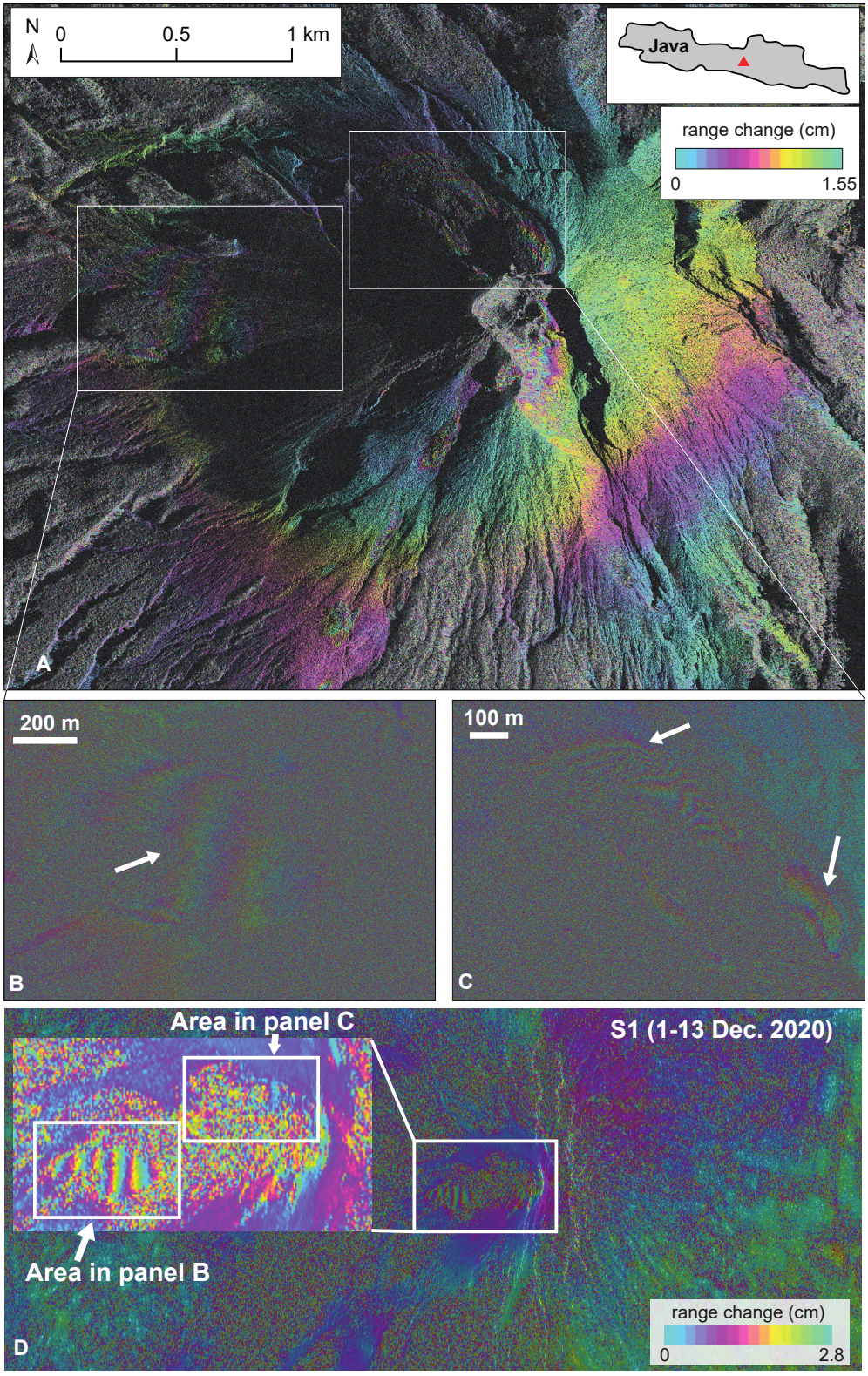

Figure 5: [A–C] Wrapped interferograms (descending orbit) made from combining SL acquisitions by TerraSAR-X on 3 December 2020, and PAZ on 7 December 2020, showing localized flank deformation at Merapi volcano, Indonesia. [A] Phase change overlain on amplitude. [B–C] Zoomed frames of areas indicated by white boxes in panel A showing only phase change and highlighting multiple areas of localized high-rate deformation (white arrows). The 4-day interval made possible by combining PAZ and TSX provided excellent temporal resolution of this deformation, which could not easily be measured using ground-based monitoring. Similar interferogram using only data from TSX is given in Poland and Zebker [2022]. [D] 12-day Sentinel-1 wrapped interferogram (descending orbit) in native radar coordinates spanning 1–13 December 2020. On the left is shown a zoom of areas covered by panel B and C. 30-m Copernicus DEM was used to remove the topographic effects.

data acquired on similar dates at Lewotolok volcano. All the Sentinel-2 data are affected by volcanic emissions that partially mask the crater area, complicating lava flow tracking (Figure 6G–L). In addition, TSX/TDX HS mode provides better resolution of the lava flows, with respect to the 20 m pixel^{-1} and the 10 m pixel^{-1} resolution of the Sentinel-2 Short-Wave Infrared (SWIR) and the optical/Near Infrared (NIR) bands, respectively.

SM data also allow for detection of the evolution of surface change in different volcanoes. For example, SM data acquired in February 2012 and in January 2013 at Raung volcano (Indonesia; Figure 7A–B) show that the small inner crater (~1 km^2) of Raung caldera became filled by newly erupted material no later than 7 January 2013 (Figure 7A–B), probably as a consequence of the eruption that ended the day before the acquisition of the image in Figure 7B [Global Volcanism Program 2022]. Figure 7C–D shows that lava flow emplacement during the eruption started on 2 October 2018, at Soputan volcano (Indonesia) as detected by SM ascending data. The potential of X-band SAR amplitude data to monitor remote volcanoes is also shown by data from Heard volcano, in the southern Indian Ocean. This volcano is usually covered by clouds, making the monitoring of its lava flows difficult using optical/thermal data. Figure 7E–F shows the growth of a narrow lava flow from March to April 2022. Thanks to the spatial resolution (~3 m pixel^{-1}) of these data, we are able to detect in detail this lava flow growth over time.

A further example of surface changes occurred in remoted volcanoes that has been possible to detect and monitor through TSX/TDX data comes from Ambae volcano (Vanuatu; Figure 8). Here SL data detected the surface changes related to intermittent activity since December 2021 through at least mid-2023, showing the formation and growth of a new cone within the caldera lake during the December 2021–August 2022 eruption (Figure 8A–D), and further surface changes associated with eruptive activity in 2023 (Figure 8E–G). SL data were also able to detect an enlargement of the inner crater (Figure 8F) immediately before one of the main paroxysms, which deposited a large amount of new material in the north part of the caldera (Figure 8H) between 4–7 April, as inferred from the timing of the ascending (Figure 8F) and the descending (Figure 8H) data.

SAR amplitude data in X-band can also be used to track lava dome growth. ??A–C shows the cycle of lava dome growth and destruction at La Soufrière Volcano (St. Vincent) detected by SL data [see further details in Dualeh et al. 2023], whereas ??D–J shows dome growth during a time span of ~7 months (May 2008 to January 2009) at Chaiten (Chile) [see further details in Delgado et al. 2022].

Finally, displacements can be calculated through pixel-offset tracking in the along-track (azimuth) and across-track (range) directions directly from the amplitudes of SAR images acquired over time. In Figure 10, we show a comparison of displacements at the caldera of Sierra Negra (Galápagos), which occurred during the second half of the 2018 eruption, detected with InSAR (LOS displacements; Figure 10A) and with pixel-offsets (across- and along-track displacements; Figure 10B–C). Results show higher displacements in the across-track than in the along-track direction (Figure 10B–C), with the magnitude of the across-track displacements comparable to those of the LOS displacements (Figure 10A–B). Near the intra-caldera faults of Sierra Negra there are some differences in the coherence of InSAR and pixel offset, with the latter remaining coherent in areas where InSAR is not coherent and vice versa (Figure 10).

3.3 Topographic changes inferred from bistatic pairs of TSX/TDX data

We used bistatic TSX/TDX pairs to evaluate topographic change related to volcanic activity at different volcanoes. In addition, we estimated the uncertainty in topographic change obtained from the bistatic data we processed to show the different thresholds of sensitivity of these data in different environments (e.g. glacial, tropical, arid) and with reference DEMs with different resolutions. To compute errors in the height change, we selected a reference area in our image that did not experience height changes and we calculated the mean value (which ideally should be close to zero) and the standard deviation of the pixels within this area [Table 2; Poland 2014; Kubanek et al. 2017]. We used reference areas larger or equal to the area affected by topographic changes, trying to select (as far as possible) areas with flat or mild topography [Kubanek et al. 2017]. Results are shown in Figure 11 and Table 2. In detail, Figure 11A shows the height change due to exogenous growth of the lava dome at Ibu volcano (Indonesia) from 2013 (time of acquisition of the Pléiades DEM used as a reference) to 2018. The resulting volume change of the dome is of $38 \pm 4 \times 10^6$ m^3 (Table 2). Areas outside the lava dome, used as references to calculate height change errors, are completely covered by vegetation, and this could explain the relatively high errors associated with the heights (Table 2). At Pacaya volcano (Guatemala; Figure 11B–C), bistatic pairs have been used to calculate the thickness of lava flows that occurred both along the volcano's flank and near the summit crater (Figure 11B–C). To better estimate the thickness of these two lava flows, we processed bistatic data acquired both before and after lava flow emplacement by using a TanDEM-X DEM acquired in 2012 to remove background (unchanging) topography and then calculating the difference between the pre- and post- lava flow emplacement bistatic pairs (Figure 11B–C). We estimated a volume of $9.30 \pm 3.19 \times 10^6$ m^3 for lava flows erupted on the flank at the beginning of January 2014 at Pacaya (Figure 11B) and of $8.76 \pm 1.36 \times 10^6$ m^3 for lavas emplaced near the summit from November 2017 to November 2019 (Figure 11C). In Figure 11D, we show how bistatic data are also able to detect topographic changes due to PDCs, tephra deposition, and destruction of part of the volcano summit during the 2015 explosive eruption of Calbuco (Chile).

Despite the high spatial resolution of the bistatic data, they sometimes do not allow detection and quantification of volcanic activity. This is the case for Sabancaya volcano (Perù), where the ascending data show no coherence within the small crater 0.14 km^2) or along the flank. The loss of coherence is partially due to the use of a SRTM DEM as a reference, since no better resolution DEMs were available, and to layover effects (with a consequent loss of information) on the western

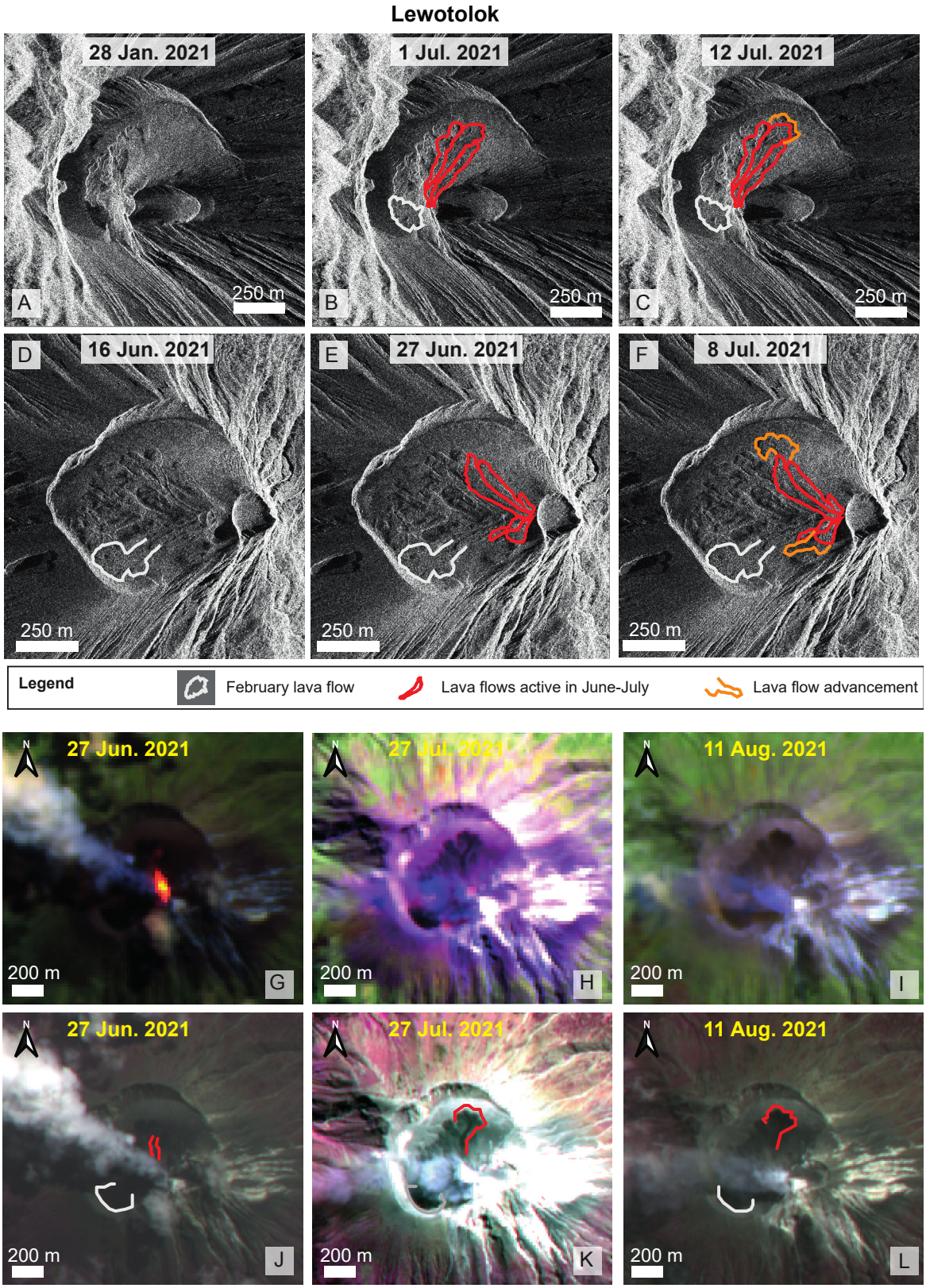

Figure 6: Surface change documented at Lewotolok volcano (Indonesia; Table 1). [A–F] High Resolution (HS mode) Synthetic Aperture Radar (SAR) backscatter data in radar coordinates from ascending [A–C] and descending [D–F] orbits showing formation of the lava flows and explosion crater during the 2021 eruption. The scenes are approximately 1 km wide. [G–L] For comparison, we show available cloud-free data from [G, H, J, K] Sentinel 2B and [I, L] Sentinel 2A taken at approximately the same time as the SAR images. [G–I] False-color images obtained by combining optical and SWIR bands (R = band 12; G = band 11; B = band 4) with a spatial resolution of ~20 m pixel^{-1} of the Short-Wave Infrared (SWIR) bands. [J–L] False color images (R = band 5; G = band 4; B = Band 3) with a spatial resolution of ~10 m pixel^{-1}.

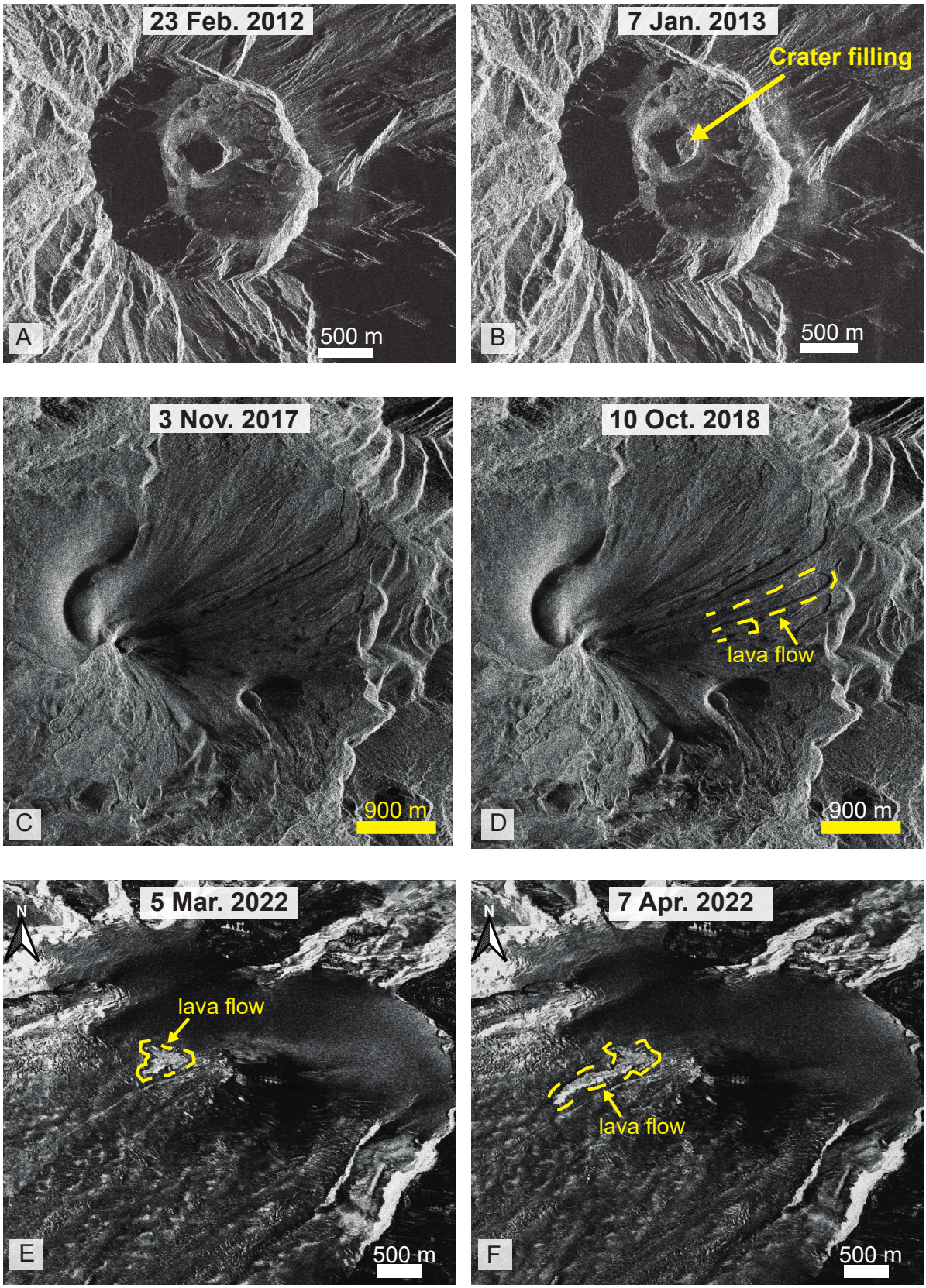

Figure 7: SAR backscatter images from [A–B] Raung caldera (Indonesia; Table 1), [C–D] Soputan volcano (Indonesia; Table 1), and [E–F] Heard Island (Australia; Table 1). [A–D] Data in radar coordinates. [E–F] Geocoded data. Descending orbit data in panels A–B and E–F and ascending orbit data in panels C–D. The location of new lava flow is labeled in D–F.

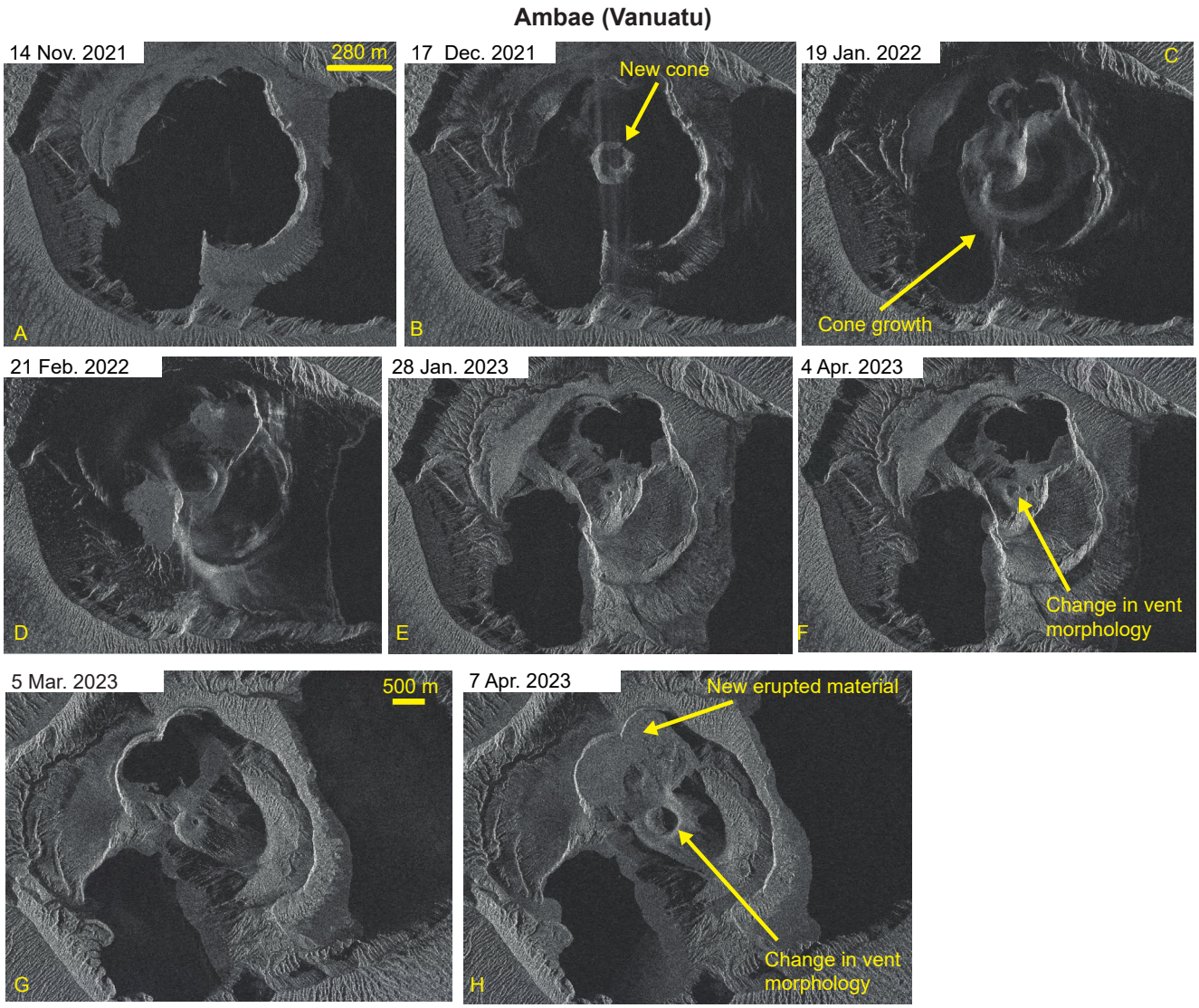

Figure 8: [A–D] SAR backscatter images (Spotlight mode; ascending orbit) of Ambae volcano showing the formation and growth of a new island within the caldera lake during the December 2021–August 2022 eruption and [E–F] the change in the inner cone morphology during the eruption that started in February 2023 and that is still ongoing as of mid 2023. [G–H] Descending SAR backscatter images (Spotlight mode) of Ambae volcano showing newly erupted material that was deposited in the north sector of the caldera during the 2023 eruption.

flank of the volcano (in the direction of the satellite's LOS; Table 2; Figure 11E), caused by the steep topography. The presence of glaciers also affects the ability to quantify the lava flow thickness from bistatic data because of partial melting of the ice due to the lava flow emplacement. This latter effect prevents a proper estimate of the lava flow thickness, since melting causes a "drop" of the ground baseline over which the lava flow spreads, which can result in a "negative" height change if the thickness of the flow is less than the depth of melted ice, as observed at Heard volcano (Figure 11F and Table 2). Similar negative topographic changes have been obtained from bistatic TSX/TDX data in Hawai'i, where lava flows from Kīlauea show a negative height change in areas where they overran heavy vegetation. This occurred because lava flows destroyed the trees that defined the pre-eruptive reference surface [Kubanek et al. 2021]. In Figure 11G, we show another topographic change from a volcano covered by snow, computing the height change from a 2021 bistatic dataset and the 30 m Copernicus DEM at Cerro Hudson (Chile). The last eruption at the volcano occurred in October 2011 [Delgado et al. 2014], with topographic change of more than 50 m due to the melting of the glacier in the interior of its caldera (Table 2).

The thicknesses of the lava flows erupted on the north flank at Sierra Negra (Galápagos) in 2018 (Figure 12) have been calculated by using both a DEM derived from Pléiades optical images subtracted from the 12 m TanDEM-X WorldDEM [Shreve and Delgado 2023], and by using bistatic TSX/TDX (CoSSC) data subtracted from the same WorldDEM (Table 2). The total bulk volume change of the 2018 lava flows estimated from the topographic change is $186.7 \pm 26.2 \times 10^6\,\mathrm{m}^3$ for the TanDEM-X–CoSSC and $193 \times 10^6\,\mathrm{m}^3$ for Pléiades–TanDEM-X. The similarity of the results, with less than 4 %

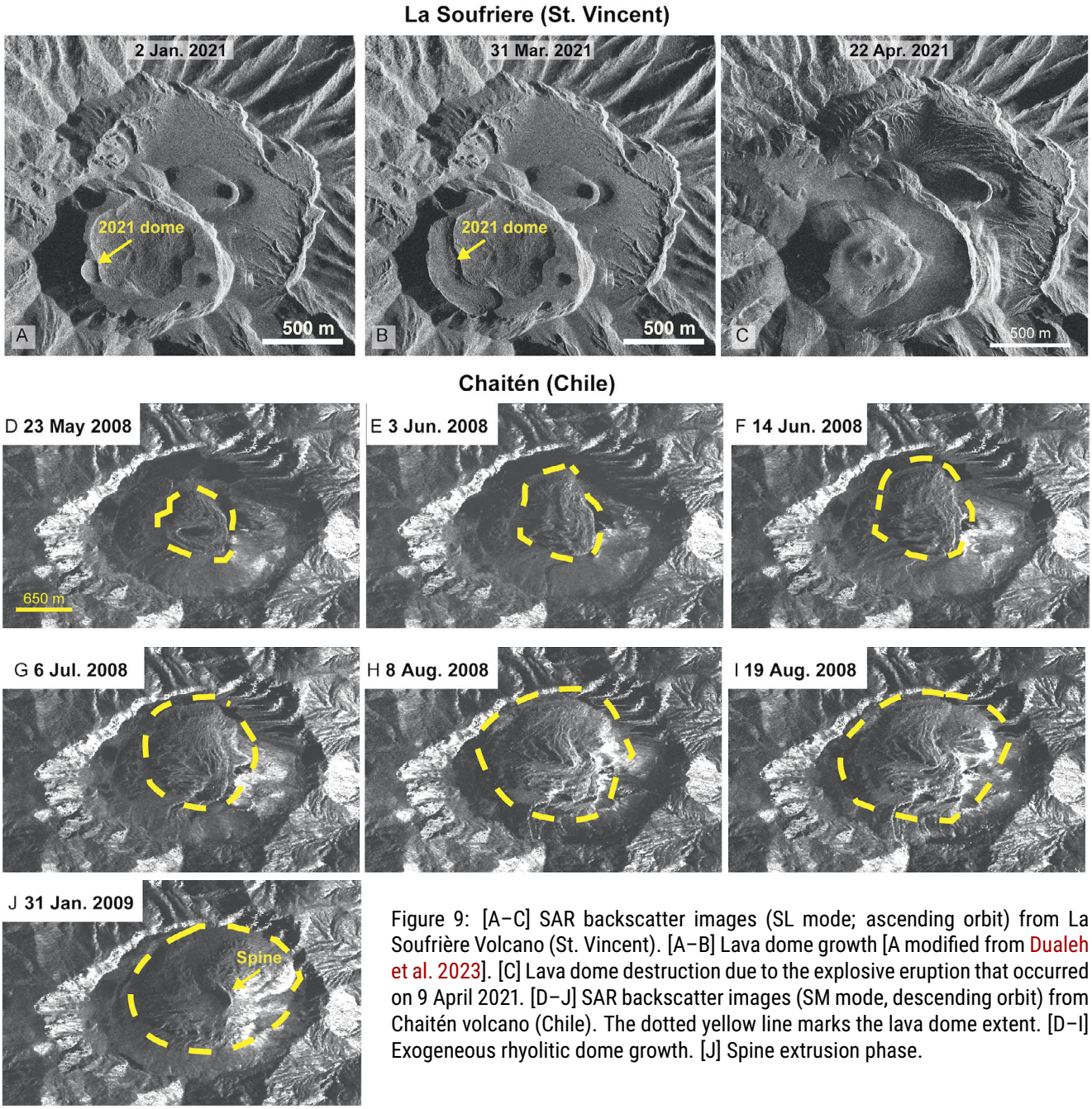

Figure 9: [A–C] SAR backscatter images (SL mode; ascending orbit) from La Soufrière Volcano (St. Vincent). [A–B] Lava dome growth [A modified from Dualeh et al. 2023]. [C] Lava dome destruction due to the explosive eruption that occurred on 9 April 2021. [D–J] SAR backscatter images (SM mode, descending orbit) from Chaitén volcano (Chile). The dotted yellow line marks the lava dome extent. [D–I] Exogeneous rhyolitic dome growth. [J] Spine extrusion phase.

difference in the volume change obtained from the bistatic TSX/TDX (CoSSC) pair and from Pléiades, further confirms the utility of bistatic TSX/TDX data to infer elevation and volume changes.

4 Discussion

Based on our work and the previous literature (Supplementary Material 1 Table S1), TSX/TDX/PAZ data provide valuable insights into volcanic processes and hazards. TSX/TDX/PAZ InSAR and SAR backscatter data are useful for anticipating eruptions [e.g. Pallister et al. 2013; Salzer et al. 2014], and InSAR has also helped to characterize volcanic unrest [e.g. Ebmeier et al. 2016; Henderson et al. 2017; MacQueen et al. 2020; Eiden et al. 2023]. The data from the satellite constellation have also been used to track co- and post- eruptive changes to better understand future hazards using InSAR, coherence change, SAR backscatter, and CoSSC-derived topography (Supplementary Material 1 Table S1).

High-resolution TSX/TDX/PAZ data have been collected and analyzed, in this study or in previous work, at 124 volcanoes (Table 1 and Supplementary Material 1 Table S1), but they could be useful at many more. Specifically, one of our primary goals is to understand if other volcanoes have not been studied with TSX/TDX/PAZ data because of (1) insufficient data, (2) poor data quality (i.e. no InSAR coherence), or (3) sufficient data and quality, but no significant changes were detected due to inadequate temporal or spatial sampling or the fact that no changes occurred. For comparison, 185 volcanoes

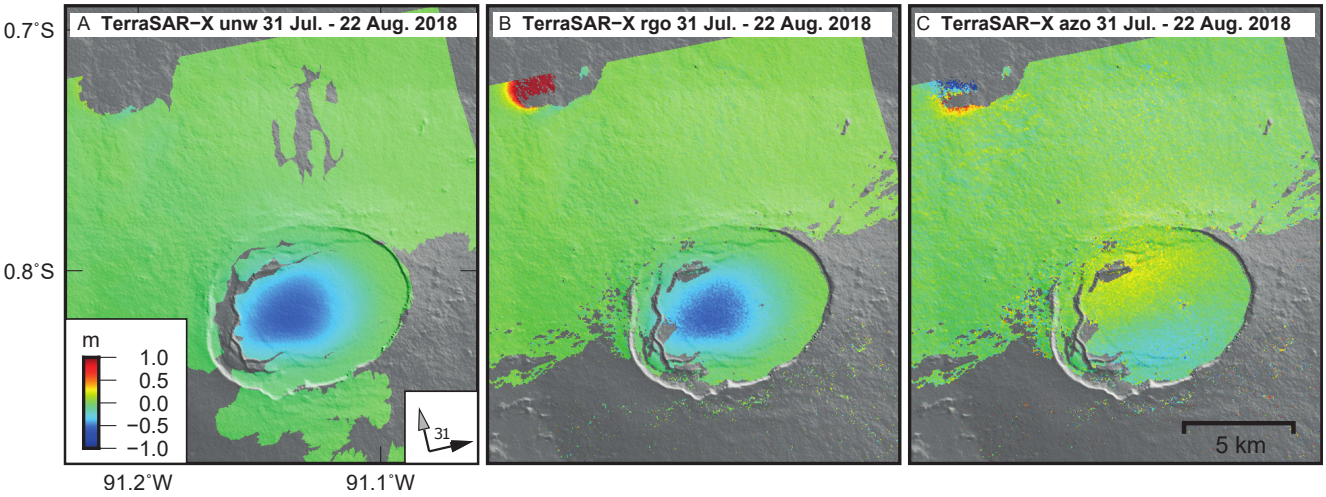

Figure 10: Displacements at Sierra Negra (Galápagos) during the final stages of the 2018 eruption. [A] LOS displacements from InSAR. Arrows point the geometry of movement and acquisition of the satellite (the incident angle is also reported). [B] across-track (range) displacements and [C] along-track (azimuth) displacements obtained through pixel-offset tracking.

Table 2: Parameters estimated from the analyzed bistatic data.

	Mean (m)[a]	Std (m)[a]	V (m^3)[b]
Ibu	1.9	5.6	$(38\pm4)\times10^6$
Calbuco	0.57	3.3	
Sabancaya	−0.03	2.34	
Heard	0.09	2.31	$(-1.65\pm0.85)\times10^6$
Cerro Hudson	1.6	7.7	
Pacaya (2014–2013)	−0.21	2.30	$(9.30\pm3.19)\times10^6$
Pacaya (Nov. 2017–Nov. 2019)	−0.75	1.89	$(8.76\pm1.36)\times10^6$
Sierra Negra[c]	−0.09	1.2	$(186.7\pm26.2)\times10^6$

[a] Mean is the mean value and Std is the standard deviation of the heights calculated in referenced areas that do not experience height changes. These parameters are used to define the height errors (see Section 3.3).
[b] V is the volume change calculated in areas that were covered by lava and that experience height change.
[c] The volume is referred only to lavas erupted on the north flank during the 2018 eruption.

have erupted during the operation of the constellation [which started on 10 July 2007; Global Volcanism Program 2022], and several hundred additional volcanoes have had some type of unrest (earthquakes, ground deformation, degassing, thermal features) without eruption [Pritchard et al. 2022a]. Other considerations, such as the latency and ease of use of the data, are important factors affecting remote sensing utility during volcanic crises [Ezquerro et al. 2023], but we do not discuss those aspects here.

During some volcanic crises the TSX/TDX/PAZ constellation acquires data regularly, providing a valuable dataset that can be used to evaluate the volcanic hazard [e.g. Pallister et al. 2013; Dualeh et al. 2023]. However, the main limitation in the use of TSX/TDX/PAZ data for most volcanoes is the lack of routine data acquisition, which inhibits its utility, generating an overall lack of data, especially before the onset of an eruption. Indeed, there are often only a few scenes per volcano, usually acquired in different imaging modes, limiting the potential use of TSX/TDX/PAZ to generate the years-long time series necessary for studying volcanic processes (e.g. volcanic unrest, lava dome growth, etc.). This often represents a limitation with respect to Cosmo-SkyMed (CSK), another X-band satellite constellation that consistently acquires data over numerous (>160) volcanoes as part of a background mission [Sacco et al. 2015]. Although all volcanoes have at least a few bistatic pairs [acquired to create the WorldDEM; Riegler et al. 2015; Wessel 2018], most erupting volcanoes lack a time series of images before, during, and after eruptions.

Within the CEOS Volcano Demonstrator regions, there are 735 subaerial volcanoes, with 193 of them having TSX/TDX Stripmap (SM) data and 68 with Spotlight (SL) data, totaling 217 volcanoes, or 29 % of the total. For comparison, of the 166 volcanoes in the USA, 66 have SM and 12 have SL for 70 unique volcanoes (42 % of the total; Figure 13). We suspect that the higher percentage of volcanoes with TSX/TDX/PAZ data in the USA compared to the CEOS area is because in

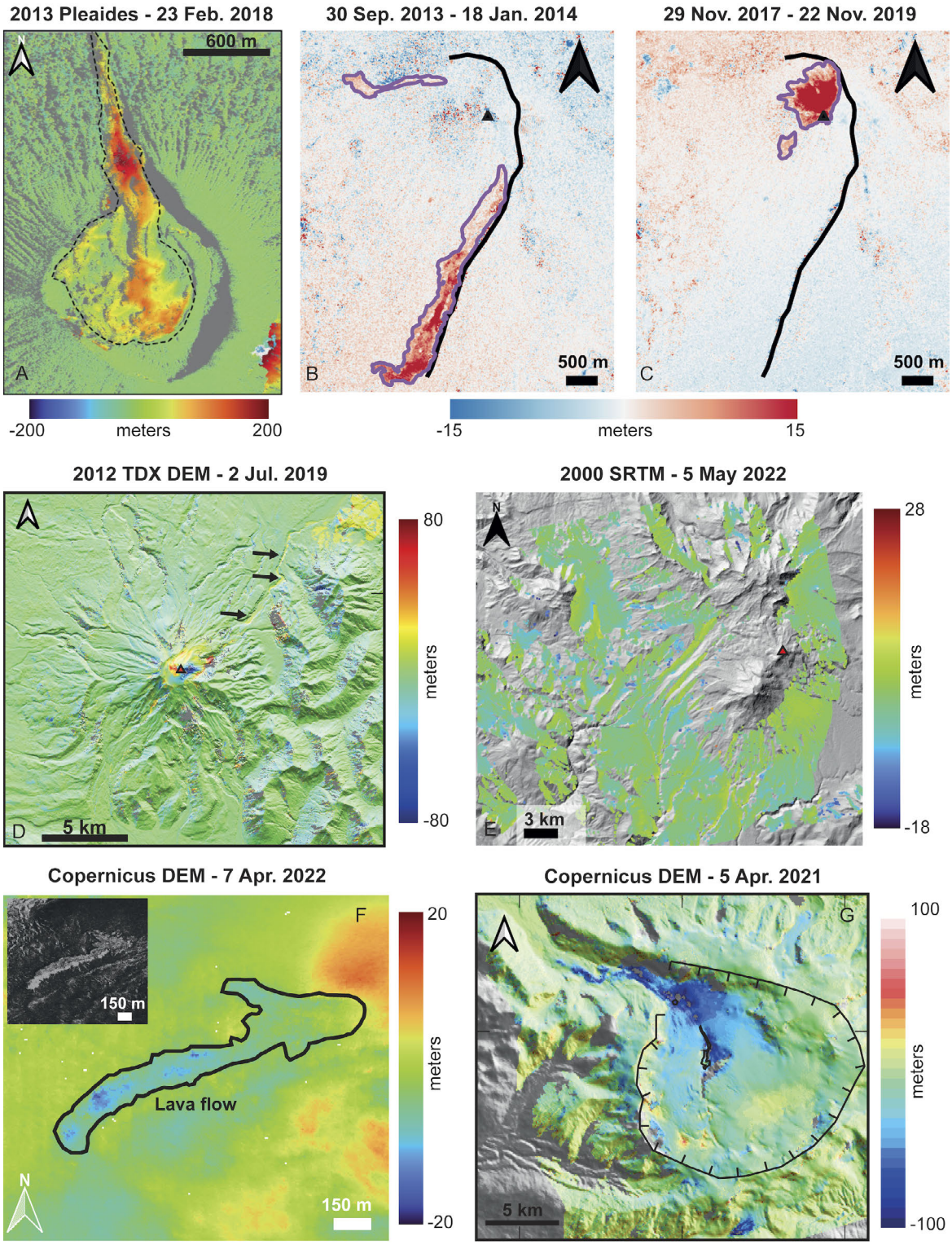

Figure 11: [A] Height changes due to lava flows (dotted line denotes area with lava flows) at Ibu (Indonesia) calculated with bistatic data with respect to a 2013 Pléiades DEM. [B–C] Height change at Pacaya (Guatemala) from bistatic data. Black triangle marks the summit vent of Pacaya, while the purple and black lines outline the lava flow and the scarp along the southern flank of Pacaya, respectively. [D] Height change at Calbuco (Chile) related to the 2015 explosive eruption with respect to a TDX DEM (acquired in 2012). Arrows point to the position of the PDCs (while the large positive signal in the NE border of the data is due to deforestation). e) Height change at Sabancaya volcano (Perù; red triangle) with respect to a SRTM DEM (acquired in 2000) showing loss of information in the area of the volcano. [F] Height changes of a lava flow at Heard volcano with respect to an upsampled (10 m pixel^{-1}) Copernicus DEM (referenced to the WGS84 ellipsoid rather than to the geoid to be consistent with the bistatic data). [G] Height change with respect to a Copernicus DEM at Cerro Hudson (Chile). The hachured line delimits the caldera area.

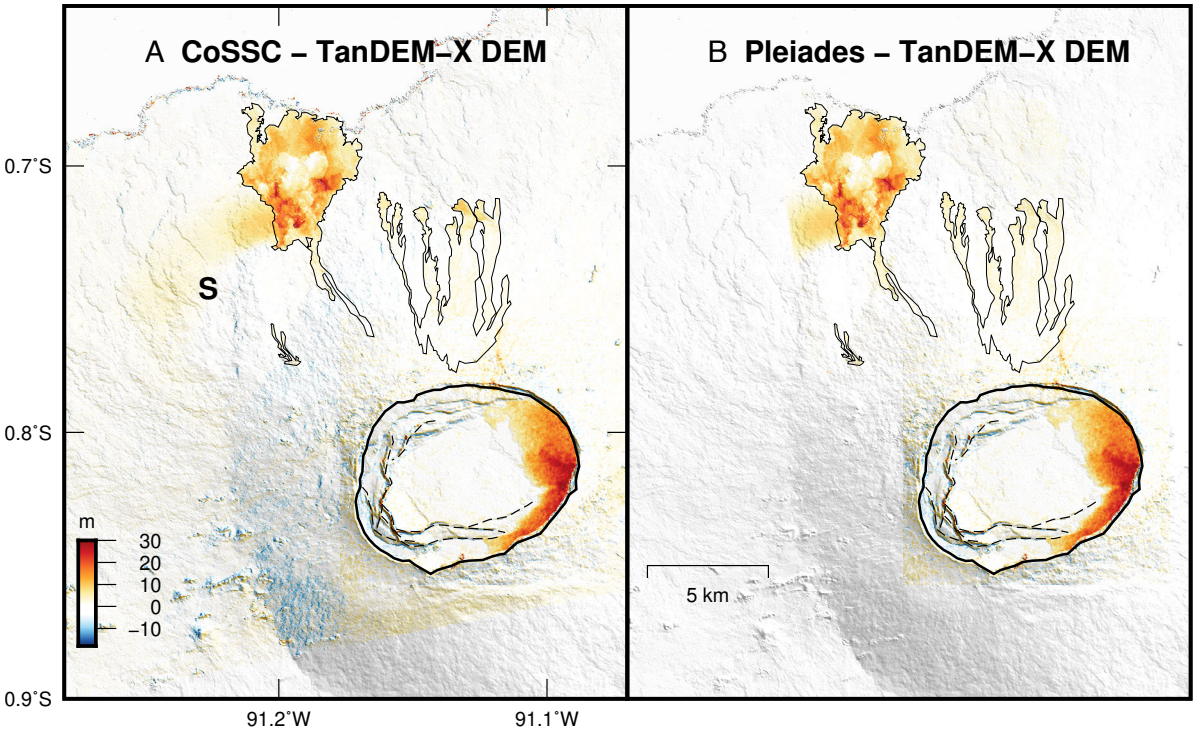

Figure 12: Elevation change at Sierra Negra, Ecuador, as a result of its 2005 and 2018 eruptions. S indicates an area of uplift due to the emplacement of a sill intrusion. The dashed black lines are faults. [A] Elevation difference between a CoSSC and the 12 m TanDEM-X. The 2018 lava flows are outlined by thin black lines on the volcano's north flank. [B] Elevation difference between a Pléiades DEM (mosaicked DEM computed from three images acquired on 28 October 2018, 6 December 2019 and 18 June 2020) and a 12 m TanDEM-X DEM acquired in 2012 [Shreve and Delgado 2023]. The elevation difference in the interior of the caldera (black line) is the lava flow erupted in 2005, whose height change has been calculated by differencing the 12 m TanDEM-X DEM acquired in 2012 and 30 m SRTM DEMs acquired in 2000 [modified from Shreve and Delgado 2023].

the USA volcanoes are more frequently tasked by scientists than volcanoes in the CEOS area. Finally, coverage by PAZ data at volcanoes is inadequate—97 % of CEOS volcanoes have no PAZ data. Of the volcanoes that do have TSX/TDX/PAZ data, the acquisitions are mostly tasked after an eruption begins, and there is often little or no pre-eruptive data in the same geometry to compare against. For example, only about half of the 36 eruptions with a Volcano Explosivity Index of 3 [Newhall and Self 1982] or larger between 2007 and 2023 in the CEOS Volcano Demonstrator regions had TSX/TDX/PAZ high spatial resolution mode (SM, SL, HS) collected before the eruption began [Global Volcanism Program 2022].

In terms of TSX/TDX/PAZ data quality at volcanoes where images are collected consistently, several criteria should be considered, given the variety of data products and modes, to understand which products are the most useful for volcano monitoring. We discuss three different categories of measurements at volcanoes mentioned in the results section in turn:

1. InSAR and coherence. Phase stability of pixels is crucial for InSAR and for measuring coherence change. This implies understanding how environmental conditions, like vegetation, precipitation, and the presence of snow/ice, cause decorrelation over time [e.g. Sica et al. 2021]. Having a short repeat time and small pixel size (among other parameters) can reduce decorrelation, but even bistatic pairs (two images acquired at the same time) can experience decorrelation. Sica et al. [2021] noted that most natural land-surface classifications are decorrelated over the 11-day repeat interval of TSX/TDX. We find that since many (but not all) volcanoes have bare rock exposed, 11-day interferograms can be coherent, especially if the perpendicular baseline is less than 100–200 m. Indeed, small perpendicular baselines usually increase the coherence of the data also in areas with low coherence (Figure 2). From this point of view, the excellent orbital control of the TSX/TDX constellation allows for the acquisition over time of SAR data with small perpendicular baselines [Buckreuss et al. 2018]. While ground deformation can be retrieved from interferogram time series with significant decorrelation using the Persistent Scatterer and similar methods [e.g. Hooper et al. 2012], we focus on single-interferogram quality, which is important in volcanic areas because the spatial complexity of deformation often requires coherence over large areas.

Integrating TSX/TDX data with PAZ data is possible to generate interferograms with temporal baselines of 4 and 7 days [Figure 5; Sica et al. 2021]) that can be more coherent than the 11-days interferograms, assuming that the perpendicular baselines are kept as small as possible. Further work is needed to determine which volcanoes require 4-, 7-, and/or 11-day repeats to maintain coherence at X-band wavelengths, or which areas cannot maintain coherence over these time intervals and require a different strategy (e.g. higher spatial resolution, <4 day temporal repeat, or different radar wave-

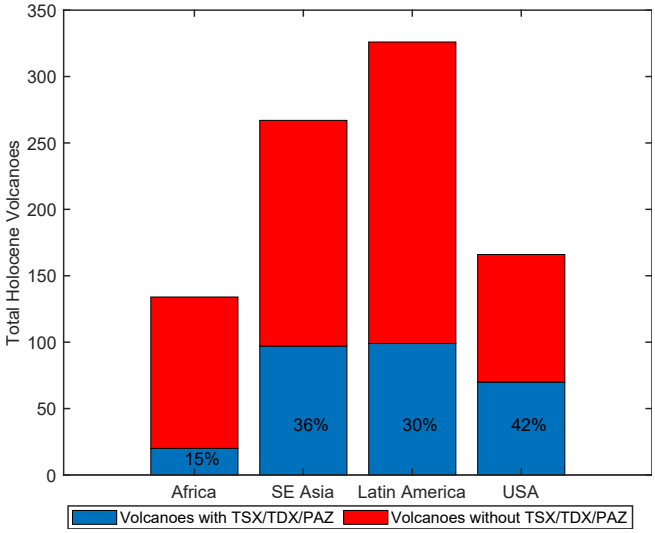

Figure 13: Number of potentially active volcanoes in the CEOS Volcano Demonstrator regions and the USA. In red are the number of volcanoes not covered by high spatial resolution (SM, HS, SL) TSX/TDX/PAZ data, while blue represents the fraction (percentage quantified in black text) having some high spatial resolution (SM, HS, SL) TSX/TDX/PAZ data [data from Pritchard et al. 2022b].

length). We find that HS interferograms can be of high quality (Figures 3 and 6; Supplementary Figures pages 52–55), especially if characterized by small temporal and perpendicular baselines, and resolve ground deformation over spatial scales of tens to hundreds of meters. We suggest further tasking in this mode over small ocean island volcanoes (e.g. Supplementary Figures pages 7–8) even beyond the enhanced acquisitions in recent years [e.g. Plank et al. 2019]. For example, at Raikoke volcano, McKee et al. [2021a] stated that "…the island is too small for the effective use of InSAR techniques…", but we suspect that the HS mode could be effective at this volcano (although only SM data have been collected to date, and no data were collected around the time of the 2019 eruption). Finally, the emplacement of volcanic products (e.g. lava or PDC) alters the scattering properties of the ground producing loss of coherence in the area covered by these products (e.g. see Supplementary Figures pages 155–158). In these cases, it is possible to use coherence maps to track the area affected by volcanic products [Zebker et al. 1996; Dietterich et al. 2012], reinforcing the need for high resolution data, like those from TSX/TDX/PAZ, to resolve the area of the volcanic products at a spatial resolution of a few meters.

2. Surface change in SAR backscatter or amplitude. To measure SAR backscatter changes at volcanoes, the key questions are whether the spatial resolution and viewing geometry are appropriate to resolve features of interest. There is no single best mode for all volcanoes, so in this case having multiple modes collected, possibly with a good number of acquisitions for each mode, is helpful to determine the best imaging characteristics for given processes and formations detectable from SAR amplitude data. Given the steep slopes of volcanoes and the SAR geometric effects of foreshortening and layover, collecting both ascending and descending orbits is usually necessary at every volcano to resolve features on both sides of the volcano (multiple examples in Supplementary Figures including Bagana, Manam, Mayon, Ulawun, Ubinas, etc.) and inside craters (e.g. Figure 6 shows that the descending orbital data allow a more detailed view into the crater of Lewotolok than the ascending orbits). Both ascending and descending data are also necessary to help resolve ground deformation in multiple directions using InSAR and/or pixel tracking [e.g. Wright et al. 2004].

A recent advance is the development of methods to quantify topographic changes directly from SAR amplitude data [Angarita et al. 2022; Dualeh et al. 2023; Smittarello et al. 2023]. These methods have been used, for example, to calculate the height and volume change of the scoria cone of Shishaldin Volcano (Alaska) from HS TSX amplitude data [Angarita et al. 2022], the growth of the lava dome at La Soufrière, (St. Vincent) from TSX and CSK amplitude data [Dualeh et al. 2023], and changes in the depth and volume of the crater of Nyiragongo volcano [Smittarello et al. 2023]. In addition, SAR amplitude data have been used to monitor the lava lake height at Nyiragongo [Barrière et al. 2022], even though these techniques have not been applied to TSX/TDX data so far. Eventually, it may be possible to calculate displacements directly from amplitude images acquired over time through pixel-tracking methods. Pixel offset has a lower sensitivity to deformation than InSAR, but it does not suffer from phase aliasing in zones of large strain [Casu et al. 2011; Shreve and Delgado 2023]. This technique has been used on TSX data to detect displacements (also in areas where InSAR failed) in volcanoes like Bárðarbunga (Iceland), Bezymianny (Russia), Merapi (Indonesia) and La Soufrière St. Vincent [Ruch et al. 2016; Himematsu et al. 2019; Mania et al. 2019; Dualeh et al. 2023; Walter 2023]. All these methods based on amplitude data testify to the importance of having high-resolution SAR data (such as TSX/TDX/PAZ data) acquired at volcanoes at a small temporal baseline to calculate topographic change and displacements during, before, and after eruptions. It is not yet possible to utilize most of these methods in near real time—necessary for hazards assessment—but continued research and development could make this goal a reality.

When considering whether to acquire HS, SL, SM, or other modes, the best criteria for evaluation may change with time. The comparison of SL and SM at several volcanoes in the Supplementary Figures can be used to help decide which mode may be best at a given volcano. For example, SM is useful to measure edifice-wide signals that can be missed by SL [e.g. Pritchard et al. 2018], whereas the higher spatial resolution modes are useful for tracking temporal changes to lava domes and flows (Figures 6–??). On the other hand, there is great value in having a consistent observation mode to develop a long time series [e.g. Valade et al. 2023]. These tradeoffs in spatial resolution, areal coverage, and temporal consistency are examples where utilizing multiple SAR constellations could be helpful [e.g. Ezquerro et al. 2023], with one set of satellites (for example, TSX/TDX/PAZ) imaging in Spotlight mode while others (e.g. CSK) collect consistent data in Stripmap [e.g. the current tasking plan at Cotopaxi volcano; Arnold et

al. 2018], or one satellite could collect ascending and the other descending. The benefit of multiple SAR constellations was observed during the 2020–2021 eruption at La Soufrière St. Vincent, where TSX data were important for the analysis of dome growth, as it was the only high-resolution SAR sensor with frequent (11-day) acquisitions throughout the eruption. This allowed for frequent and repeated observations of the lava dome, which complemented the temporally frequent but lower resolution Sentinel-1 data and the high-resolution but infrequently acquired CSK data [Dualeh et al. 2023]. Data from multiple SAR constellations could provide benefits for other categories of measurements (e.g. InSAR).

3. Topographic Change from bistatic data. The TSX/TDX bistatic pairs are an important day/night and all-weather dataset for measuring topographic change that complement optical measurements that have better vertical precision but can be obscured by clouds [Plank et al. 2023]. Even though bistatic pairs are acquired at the same time, their interferograms can have low coherence in some areas [Figure 11E; Sica et al. 2021]. Noisy scenes from bistatic pairs can have both a small separation between the TSX and TDX satellites (small B_perp), giving them less sensitivity to topography, and a large B_perp, making them susceptible to volume scattering mainly due to vegetation [e.g. Sica et al. 2021; Zink et al. 2021]. Other sources of error that can cause a loss of information are geometric decorrelations [e.g. shadow, layover and grazing incidence; e.g. Kubanek et al. 2015b] and volume decorrelation due to radar penetration phenomena [e.g. highly vegetated or snow/ice-covered regions; Zink et al. 2021]. Updated high spatial resolution DEMs of volcanoes during eruptions are critical for using InSAR to measure ground deformation. For this reason, as well as the need for updated DEMs for hazard forecasts from lava flows, lahars, dome collapse, etc., targeted daily observations are helpful to measure topographic change for erupting volcanoes [Bally 2013], which will require multiple types of satellites, including bistatic SAR like TSX/TDX or the future proposed TanDEM-L (DLR) and Harmony (ESA) missions [Kubanek et al. 2021; Plank et al. 2023]. Bistatic pairs from the TSX/TDX mission have been used to measure topographic change associated with lava flows and domes, and even pyroclastic flows [Albino et al. 2020], although sometimes loss of information/coherence owing to factors discussed above prevented detection of topographic change that was known to have occurred through other techniques [Pritchard et al. 2018]. Greater coverage and the capability to use higher spatial resolution modes like HS or SL for bistatic TSX/TDX pairs would be helpful to further improve the applicability of bistatic data.

To maximize the potential of TSX/TDX/PAZ data, which have a spatial resolution of 3 m pixel^{-1} or better, high-resolution Digital Elevation Models are needed to correct topographic distortions and accurately georeference the products without experiencing a significant loss of resolution and of coherence [e.g. Bemelmans et al. 2023]. For the InSAR products, displacement cannot be resolved when the displacement between two adjacent pixels exceeds half the radar wavelength [e.g. Michel et al. 1999], and so high spatial resolution DEMs are critical, especially for areas with large displacements focused in small areas, like in volcanic craters [e.g. Richter et al. 2013; Bemelmans et al. 2023]. Neither high spatial resolution DEMs nor high spatial resolution SAR data are freely available over all volcanoes. Another limitation is that high spatial resolution DEMs are not always updated (e.g. WorldDEM was acquired in 2012), while volcanoes are dynamic systems that can experience rapid topographic changes that completely alter their morphology [e.g. the 2018 caldera collapse at Kīlauea; Lundgren et al. 2019]. To maximize the potential of high spatial resolution SAR data, such as TSX/TDX/PAZ data, it is therefore important to have access to updated high-resolution DEMs [e.g. Pléiades, WorldDEM and bistatic TSX/TDX pairs, UAV-based photogrammetry, and Lidar DEMs; Bernard et al. 2012; Kolzenburg et al. 2016; Wessel 2018; James et al. 2020].

5 Conclusions

The long-lived TSX/TDX and now PAZ constellation has been extremely useful for studying volcanic activity worldwide within the framework of its design(global DEM and semi-commercial applications [Buckreuss et al. 2018]). TSX/TDX/PAZ can provide measurements of volcanic deformation and surface change that are critical for monitoring unrest and forecasting eruptions, but the background observations that make these data most useful for volcano applications are currently available for less than 30 % of the volcanoes worldwide. Most volcanoes on Earth (>800) need images annually or every few years, but the most active and hazardous (about 200 volcanoes) need observations as frequently as possible (daily to every few days) from TSX/TDX/PAZ and other satellites to maintain InSAR coherence and record geomorphic changes [Pritchard et al. 2022a]. Because there are several other SAR constellations in orbit (for example, CSK, Sentinel-1, RCM, ICEYE, Capella Space, Umbra), further work is needed to determine which of the 200 or so most hazardous volcanoes need the 4–11 day TSX/TDX/PAZ acquisitions as opposed to acquisitions by other satellite systems. To track possibly subtle changes in ground deformation before an eruption, a time series of routine acquisitions of high spatial resolution complex imagery (e.g. SM, SL, HS) in the same geometry and format, and with small perpendicular baselines, is required for InSAR. Currently, only a fraction (<30 %) of CEOS demonstrator volcanoes are receiving adequate background observations from TSX/TDX/PAZ (Figure 13). In addition to tasking volcanoes during eruptive crises, a quota of background acquisitions could be allocated to anticipate future eruptions. It would also be advantageous to coordinate TSX/TDX/PAZ global volcano acquisition strategies with other SAR constellations through a Volcano Space Task Group [Pritchard et al. 2022a] so that each set of satellites collect data in complementary modes (ascending vs. descending, incidence angle, SM vs. SL, etc.). The TSX/TDX mission has already significantly exceeded its designed lifetime (5.5 yr^{-1}), even though it is expected to remain operational for a few more years [Buckreuss et al. 2018; Bojarski et al. 2021]. Future missions that continue the capacity of this successful constellation, especially in terms of acquisition of bistatic data, would benefit for volcanological applications.

Author Contributions

M. Pritchard coordinated the project and wrote the first draft together with F. Galetto. F. Galetto, E. Dualeh, and M. Poland processed most of the data and generated most of the reports. F. Delgado processed the data for Wolf, Sierra Negra, Chaitén, Calbuco, and Cerro Hudson and wrote the associated text. T. Shreve processed the data for Ibu and Ambrym. I. Hamling processed the data for Ambae. J. Gonzalez Santana processed the data for Pacaya and wrote the associated report. J-L. Froger processed the data of Karthala and Piton de la Fournaise and generated the associated reports. All Authors contributed ideas and input to the research and writing of the paper.

Acknowledgements

We acknowledge the CEOS Volcano Demonstrator project and the space agencies and companies that provided data: the German Space Agency and Airbus for TSX/TDX data and CoSSCs, the Spanish Space Agency for PAZ and the European Space Agency for Sentinel data. F. Galetto and M. Pritchard were supported by grant 80NSSC21K0842 issued through NASA's Science Mission Directorate's Earth Science Division. J. Gonzalez Santana and C. Wauthier were supported by NASA's ESI grant 80NSSC20K0490 and FINESST grant 80NSSC20K1632. S. K. Ebmeier is funded by a NERC Independent Research Fellowship (NE/R015546/1). E. Dualeh, J. Biggs, and S. K. Ebmeier are supported by NERC–BGS COMET. T. Shreve acknowledges Raphaël Grandin for access to the Ibu data through DLR project number XTI_GEOL6544, and Pléiades project number ISIS 2017-253.

We are grateful to two anonymous reviewers and to the USGS reviewer for their helpful comments and suggestions that improved the quality of this manuscript.

F. Galetto is grateful to Diego Lobos Lillo for the help with the scripts for processing bistatic pair data.

Any use of trade, firm, or product names is for descriptive purposes only and does not imply endorsement by the U.S. Government.

Data Availability

Additional references in Supplementary Material 1 Table S1 are also reported in the main text References. The Supplementary Material 1 Table S1 and the Supplementary Figures File with all the Supplementary Figures, as well as all the reports making up the Supplementary Figures File have also been deposited in a permanent data repository and are available at https://osf.io/35xud/

GVP database available at: https://doi.org/10.5479/si.GVP.VOTW5-2022.5.0

Eoweb GeoPortal is available at: https://eoweb.dlr.de/guestegp/main#mainWindowtabExplore

Copyright Notice

References

Albino, F., J. Biggs, R. Escobar-Wolf, A. Naismith, M. Watson, J. C. Phillips, and G. A. Chigna Marroquin (2020). "Using TanDEM-X to measure pyroclastic flow source location, thickness and volume: Application to the 3rd June 2018 eruption of Fuego volcano, Guatemala". *Journal of Volcanology and Geothermal Research* 406, page 107063. ISSN: 0377-0273. DOI: 10.1016/j.jvolgeores.2020.107063.

Albino, F., B. Smets, N. d'Oreye, and F. Kervyn (2015). "High-resolution TanDEM-X DEM: An accurate method to estimate lava flow volumes at Nyamulagira Volcano (D. R. Congo)". *Journal of Geophysical Research: Solid Earth* 120(6), pages 4189–4207. ISSN: 2169-9356. DOI: 10.1002/2015jb011988.

Aldeghi, Carn, Escobar-Wolf, and Groppelli (2019). "Volcano monitoring from space using high-cadence Planet CubeSat images applied to Fuego Volcano, Guatemala". *Remote Sensing* 11(18), page 2151. ISSN: 2072-4292. DOI: 10.3390/rs11182151.

Ali, S. T., J. Akerley, E. C. Baluyut, M. Cardiff, N. C. Davatzes, K. L. Feigl, W. Foxall, D. Fratta, R. J. Mellors, P. Spielman, H. F. Wang, and E. Zemach (2016). "Time-series analysis of surface deformation at Brady Hot Springs geothermal field (Nevada) using interferometric synthetic aperture radar". *Geothermics* 61, pages 114–120. ISSN: 0375-6505. DOI: 10.1016/j.geothermics.2016.01.008.

Angarita, M., R. Grapenthin, S. Plank, F. J. Meyer, and H. Dietterich (2022). "Quantifying large-scale surface change using SAR amplitude images: Crater morphology changes during the 2019–2020 Shishaldin Volcano eruption". *Journal of Geophysical Research: Solid Earth* 127(8). ISSN: 2169-9356. DOI: 10.1029/2022jb024344.

Arnold, D. W. D., J. Biggs, K. Anderson, S. Vallejo Vargas, G. Wadge, S. K. Ebmeier, M. F. Naranjo, and P. Mothes (2017). "Decaying lava extrusion rate at El Reventador Volcano, Ecuador, measured using high-resolution satellite radar". *Journal of Geophysical Research: Solid Earth* 122(12), pages 9966–9988. DOI: 10.1002/2017JB014580.

Arnold, D. W. D., J. Biggs, G. Wadge, and P. Mothes (2018). "Using satellite radar amplitude imaging for monitoring syn-eruptive changes in surface morphology at an ice-capped stratovolcano". *Remote Sensing of Environment* 209, pages 480–488. ISSN: 0034-4257. DOI: 10.1016/j.rse.2018.02.040.

Bally, P., editor (2013). *Satellite Earth Observation for Geohazard Risk Management - The Santorini Conference - Santorini, Greece, 21–23 May 2012. ESA Publication STM-282*. DOI: 10.5270/esa-geo-hzrd-2012.

Barrière, J., N. d'Oreye, A. Oth, H. Geirsson, N. Mashagiro, J. B. Johnson, B. Smets, S. Samsonov, and F. Kervyn (2018). "Single-station seismo-acoustic monitoring of Nyiragongo's lava lake activity (D.R. Congo)". *Frontiers in Earth Science* 6. ISSN: 2296-6463. DOI: 10.3389/feart.2018.00082.

Barrière, J., N. d'Oreye, B. Smets, A. Oth, L. Delhaye, J. Subira, N. Mashagiro, D. Derauw, D. Smittarello, A. M. Syavulisembo, and F. Kervyn (2022). "Intra-crater eruption dynamics at Nyiragongo (D.R. Congo), 2002–2021". *Journal of Geophysical Research: Solid Earth* 127(4). ISSN: 2169-9356. DOI: 10.1029/2021jb023858.

Bemelmans, M. J. W., J. Biggs, M. Poland, J. Wookey, S. K. Ebmeier, A. K. Diefenbach, and D. Syahbana (2023). "High-resolution InSAR reveals localized pre-eruptive deformation inside the crater of Agung Volcano, Indonesia". *Journal of Geophysical Research: Solid Earth* 128(5). ISSN: 2169-9356. DOI: 10.1029/2022jb025669.

Bernard, M., D. Decluseau, L. Gabet, and P. Nonin (2012). "3D capabilities of Pléiades satellite". *The International Archives of the Photogrammetry, Remote Sensing and Spatial Information Sciences* XXXIX-B3, pages 553–557. ISSN: 2194-9034. DOI: 10.5194/isprsarchives-xxxix-b3-553-2012.

Bernard, O. and C. Bouvet de Maisonneuve (2020). "Controls on eruption style at Rabaul, Papua New Guinea—Insights from microlites, porosity and permeability measurements". *Journal of Volcanology and Geothermal Research* 406, page 107068. ISSN: 0377-0273. DOI: 10.1016/j.jvolgeores.2020.107068.

Bird, P. (2003). "An updated digital model of plate boundaries". *Geochemistry, Geophysics, Geosystems* 4(3). ISSN: 1525-2027. DOI: 10.1029/2001gc000252.

Bojarski, A., M. Bachmann, J. Boer, T. Kraus, C. Wecklich, U. Steinbrecher, N. Tous-Ramon, K. Schmidt, P. Klenk, C. Grigorov, M. Schwerdt, and M. Zink (2021). "TanDEM-X long-term system performance after 10 years of operation". *IEEE Journal of Selected Topics in Applied Earth Observations and Remote Sensing* 14, pages 2522–2534. ISSN: 2151-1535. DOI: 10.1109/jstars.2021.3055546.

Bredemeyer, S., F.-G. Ulmer, T. Hansteen, and T. Walter (2018). "Radar path delay effects in volcanic gas plumes: The case of Láscar Volcano, Northern Chile". *Remote Sensing* 10(10), page 1514. ISSN: 2072-4292. DOI: 10.3390/rs10101514.

Buckreuss, S., B. Schättler, T. Fritz, J. Mittermayer, R. Kahle, E. Maurer, J. Böer, M. Bachmann, F. Mrowka, E. Schwarz, H. Breit, and U. Steinbrecher (2018). "Ten years of TerraSAR-X operations". *Remote Sensing* 10(6), page 873. ISSN: 2072-4292. DOI: 10.3390/rs10060873.

Castro, J. M., B. Cordonnier, C. I. Schipper, H. Tuffen, T. S. Baumann, and Y. Feisel (2016). "Rapid laccolith intrusion driven by explosive volcanic eruption". *Nature Communications* 7(1). ISSN: 2041-1723. DOI: 10.1038/ncomms13585.

Casu, F., A. Manconi, A. Pepe, and R. Lanari (2011). "Deformation time-series generation in areas characterized by large displacement dynamics: The SAR amplitude pixel-offset SBAS technique". *IEEE Transactions on Geoscience and Remote Sensing* 49(7), pages 2752–2763. ISSN: 1558-0644. DOI: 10.1109/tgrs.2010.2104325.

Chen, Y., D. Remy, J.-L. Froger, A. Peltier, N. Villeneuve, J. Darrozes, H. Perfettini, and S. Bonvalot (2017). "Long-term ground displacement observations using InSAR and GNSS at Piton de la Fournaise volcano between 2009 and 2014". *Remote Sensing of Environment* 194, pages 230–247. ISSN: 0034-4257. DOI: 10.1016/j.rse.2017.03.038.

Chorowicz, J., B. Deffontaines, D. Huaman-Rodrigo, R. Guillande, F. Leguern, and J. C. Thouret (1992). "SPOT satellite monitoring of the eruption of Nevado Sabancaya volcano (Southern Peru)". *Remote Sensing of Environment* 42(1), pages 43–49. ISSN: 0034-4257. DOI: 10.1016/0034-4257(92)90066-s.

Cong, X., M. Eineder, S. Gernhardt, and R. Bamler (2011). "Detection of the volcanic deformation with multi-stack persistent scatterer interferometry using TerraSAR-X data". *EGU General Assembly*.

Cong, X., M. Eineder, and T. Fritz (2012). "Atmospheric delay compensation in differential SAR interferometry for volcanic deformation monitoring—study case: El Hierro". *2012 IEEE International Geoscience and Remote Sensing Symposium*. IEEE. DOI: 10.1109/igarss.2012.6350563.

Dai, C., I. M. Howat, J. T. Freymueller, Z. Lu, S. Vijay, A. K. Liljedahl, M. K. Ward Jones, H. Bergstedt, and E. Lev (2022). "Quantifying mass flows at Mt. Cleveland, Alaska between 2001 and 2020 using satellite photogrammetry". *Journal of Volcanology and Geothermal Research* 429, page 107614. ISSN: 0377-0273. DOI: 10.1016/j.jvolgeores.2022.107614.

De Paolo, E., T. Walter, E. Zorn, D. Coppola, M. Laiolo, F. Massimetti, and M. Battaglia (2019). "Lateral lava dome growth monitoring at Nevado del Ruiz Arenas crater using TerraSAR-X amplitude imagery". *EGU General Assembly*, 9502.

De Rauw, D., F. Kervyn, N. d'Oreye, B. Smets, F. Albino, and C. Barbier (2015). "Split-band interferometric SAR processing using TanDEM-X data". *FRINGE 2015*. Frascati, Italy.

DeGrandpre, K. G., J. D. Pesicek, Z. Lu, H. R. DeShon, and D. C. Roman (2019). "High rates of inflation during a noneruptive episode of seismic unrest at Semisopochnoi Volcano, Alaska in 2014–2015". *Geochemistry, Geophysics, Geosystems* 20(12), pages 6163–6186. ISSN: 1525-2027. DOI: 10.1029/2019gc008720.

Delgado, F., R. Contreras-Arratia, and S. Samsonov (2022). "Magma buoyancy drives rhyolitic eruptions: A tale from the VEI 5 2008–2009 Chaitén eruption (Chile) from seismological and geodetic data". *Earth and Planetary Science Letters* 590, page 117564. ISSN: 0012-821X. DOI: 10.1016/j.epsl.2022.117564.

Delgado, F. and R. Grandin (2021). "Dynamics of episodic magma injection and migration at Yellowstone Caldera: Revisiting the 2004–2009 episode of caldera uplift with InSAR and GPS data". *Journal of Geophysical Research: Solid Earth* 126(8). ISSN: 2169-9356. DOI: 10.1029/2021jb022341.

Delgado, F., J. Kubanek, K. Anderson, P. Lundgren, and M. Pritchard (2019a). "Physicochemical models of effusive rhyolitic eruptions constrained with InSAR and DEM data: A case study of the 2011–2012 Cordón Caulle eruption". *Earth and Planetary Science Letters* 524, page 115736. ISSN: 0012-821X. DOI: 10.1016/j.epsl.2019.115736.

Delgado, F., M. Poland, J. Biggs, S. Ebmeier, E. Sansosti, P. Lundgren, C. Wauthier, S. Henderson, M. Pritchard, F. Amelung, and S. Zoffoli (2019b). "Lessons learned from the CEOS volcano pilot in Latin American and the ongoing volcano demonstrator project". *EGU General Assembly*.

Delgado, F., M. Pritchard, R. Lohman, and J. A. Naranjo (2014). "The 2011 Hudson volcano eruption (Southern Andes, Chile): Pre-eruptive inflation and hotspots observed with InSAR and thermal imagery". *Bulletin of Volcanology* 76(5). ISSN: 1432-0819. DOI: 10.1007/s00445-014-0815-9.

Delgado, F., M. E. Pritchard, S. Ebmeier, P. González, and L. Lara (2017). "Recent unrest (2002–2015) imaged by space geodesy at the highest risk Chilean volcanoes: Villarrica, Llaima, and Calbuco (Southern Andes)". *Journal of Volcanology and Geothermal Research* 344, pages 270–288. ISSN: 0377-0273. DOI: 10.1016/j.jvolgeores.2017.05.020.

Dietterich, H. R., S. M. Plank, and M. W. Loewen (2023). "Multi-sensor remote sensing of effusive eruption dynamics and lava flow morphology at Great Sitkin Volcano, Alaska". *IAVCEI Scientific Assembly*, 272.

Dietterich, H. R., M. P. Poland, D. A. Schmidt, K. V. Cashman, D. R. Sherrod, and A. T. Espinosa (2012). "Tracking lava flow emplacement on the east rift zone of Kīlauea, Hawai'i, with synthetic aperture radar coherence". *Geochemistry, Geophysics, Geosystems* 13(5). ISSN: 1525-2027. DOI: 10.1029/2011gc004016.

Dirscherl, M. and C. Rossi (2018). "Geomorphometric analysis of the 2014–2015 Bárðarbunga volcanic eruption, Iceland". *Remote Sensing of Environment* 204, pages 244–259. ISSN: 0034-4257. DOI: 10.1016/j.rse.2017.10.027.

Dualeh, E. W., S. K. Ebmeier, T. J. Wright, F. Albino, A. Naismith, J. Biggs, P. A. Ordoñez, R. M. Boogher, and A. Roca (2021). "Analyzing explosive volcanic deposits from satellite-based radar backscatter, Volcán de Fuego, 2018". *Journal of Geophysical Research: Solid Earth* 126(9). ISSN: 2169-9356. DOI: 10.1029/2021jb022250.

Dualeh, E. W., S. K. Ebmeier, T. J. Wright, M. P. Poland, R. Grandin, A. J. Stinton, M. Camejo-Harry, B. Esse, and M. Burton (2023). "Rapid pre-explosion increase in dome extrusion rate at La Soufrière, St. Vincent quantified from synthetic aperture radar backscatter". *Earth and Planetary Science Letters* 603, page 117980. ISSN: 0012-821X. DOI: 10.1016/j.epsl.2022.117980.

Ducrocq, C., H. Geirsson, T. Árnadóttir, D. Juncu, V. Drouin, G. Gunnarsson, B. R. Kristjánsson, F. Sigmundsson, S. Hreinsdóttir, S. Tómasdóttir, and H. Blanck (2021). "Inflation–deflation episodes in the Hengill and Hrómundartindur volcanic complexes, SW Iceland". *Frontiers in Earth Science* 9. ISSN: 2296-6463. DOI: 10.3389/feart.2021.725109.

Dumont, Q., V. Cayol, J.-L. Froger, and A. Peltier (2022). "22 years of satellite imagery reveal a major destabilization structure at Piton de la Fournaise". *Nature Communications* 13(1). ISSN: 2041-1723. DOI: 10.1038/s41467-022-30109-w.

Dumont, S., F. Sigmundsson, M. M. Parks, V. J. P. Drouin, G. B. M. Pedersen, I. Jónsdóttir, Á. Höskuldsson, A. Hooper, K. Spaans, M. Bagnardi, M. T. Gudmundsson, S. Barsotti, K. Jónsdóttir, T. Högnadóttir, E. Magnússon, Á. R. Hjartardóttir, T. Dürig, C. Rossi, and B. Oddsson (2018). "Integration of SAR data into monitoring of the 2014–2015 Holuhraun eruption, Iceland: Contribution of the Icelandic Volcanoes Supersite and the FutureVolc projects". *Frontiers in Earth Science* 6. ISSN: 2296-6463. DOI: 10.3389/feart.2018.00231.

Ebmeier, S. K., J. R. Elliott, J.-M. Nocquet, J. Biggs, P. Mothes, P. Jarrín, M. Yépez, S. Aguaiza, P. Lundgren, and S. V. Samsonov (2016). "Shallow earthquake inhibits unrest near Chiles–Cerro Negro volcanoes, Ecuador–Colombian border". *Earth and Planetary Science Letters* 450, pages 283–291. ISSN: 0012-821X. DOI: 10.1016/j.epsl.2016.06.046.

Eiden, E., P. MacQueen, S. Henderson, and M. Pritchard (2023). "Multiple spatial and temporal scales of deformation from geodetic monitoring point to active transcrustal magma system at Uturuncu volcano, Bolivia". *Geosphere* 19(2), pages 370–382. ISSN: 1553-040X. DOI: 10.1130/ges02520.1.

Eineder, M., C. Minet, P. Steigenberger, X. Cong, and T. Fritz (2011). "Imaging geodesy—Toward centimeter-level ranging accuracy with TerraSAR-X". *IEEE Transactions on Geoscience and Remote Sensing* 49(2), pages 661–671. ISSN: 1558-0644. DOI: 10.1109/tgrs.2010.2060264.

Eugenio, F., J. Martin, J. Marcello, and E. Fraile-Nuez (2014). "Environmental monitoring of El Hierro Island submarine volcano, by combining low and high resolution satellite imagery". *International Journal of Applied Earth Observation and Geoinformation* 29, pages 53–66. ISSN: 1569-8432. DOI: 10.1016/j.jag.2013.12.009.

Ezquerro, P., G. Bru, I. Galindo, O. Monserrat, J. C. García-Davalillo, N. Sánchez, I. Montoya, R. Palamà, R. M. Mateos, R. Pérez-López, E. González-Alonso, R. Grandin, C. Guardiola-Albert, J. López-Vinielles, J. A. Fernández-Merodo, G. Herrera, and M. Béjar-Pizarro (2023). "Analysis of SAR-derived products to support emergency management during volcanic crisis: La Palma case study". *Remote Sensing of Environment* 295, page 113668. ISSN: 0034-4257. DOI: 10.1016/j.rse.2023.113668.

Farr, T. G., P. A. Rosen, E. Caro, R. Crippen, R. Duren, S. Hensley, M. Kobrick, M. Paller, E. Rodriguez, L. Roth, D. Seal, S. Shaffer, J. Shimada, J. Umland, M. Werner, M. Oskin, D. Burbank, and D. Alsdorf (2007). "The Shuttle Radar Topography Mission". *Reviews of Geophysics* 45(2). ISSN: 1944-9208. DOI: 10.1029/2005rg000183.

Feigl, K. L., H. Le Mével, S. Tabrez Ali, L. Córdova, N. L. Andersen, C. DeMets, and B. S. Singer (2013). "Rapid uplift in Laguna del Maule volcanic field of the Andean Southern Volcanic zone (Chile) 2007–2012". *Geophysical Journal International* 196(2), pages 885–901. ISSN: 0956-540X. DOI: 10.1093/gji/ggt438.

Flynn, L. P., A. J. Harris, and R. Wright (2001). "Improved identification of volcanic features using Landsat 7 ETM+". *Remote Sensing of Environment* 78(1–2), pages 180–193. ISSN: 0034-4257. DOI: 10.1016/s0034-4257(01)00258-9.

Francis, P. and S. De Silva (1989). "Application of the Landsat Thematic Mapper to the identification of potentially active volcanoes in the central Andes". *Remote Sensing of Environment* 28, pages 245–255. ISSN: 0034-4257. DOI: 10.1016/0034-4257(89)90117-x.

Geirsson, H., M. M. Parks, B. G. Ofeigsson, V. Drouin, S. Li, F. Sigmundsson, T. Árnadóttir, A. R. Hjartardottir, M. Lárentínusdóttir, P. Einarsson, P. Schmidth, F. Pálsson, A. Hooper, and K. Jónsdóttir (2018). "Reawakening of the (Öræfajökull) volcano in (Iceland): deformation signals of stress triggers and intrusive activity". *EGU General Assembly*, 15438.

Global Volcanism Program (2022). *Volcanoes of the World (v. 4.10.1; 14 July 2021). [Database]. Distributed by Smithsonian Institution, compiled by Venzke, E.* DOI: 10.5479/si.gvp.votw5-2022.5.0.

Goitom, B., C. Oppenheimer, J. O. S. Hammond, R. Grandin, T. Barnie, A. Donovan, G. Ogubazghi, E. Yohannes, G. Kibrom, J. M. Kendall, S. A. Carn, D. Fee, C. Sealing, D. Keir, A. Ayele, J. Blundy, J. Hamlyn, T. Wright, and S. Berhe (2015). "First recorded eruption of Nabro volcano, Eritrea, 2011". *Bulletin of Volcanology* 77(10). ISSN: 1432-0819. DOI: 10.1007/s00445-015-0966-3.

Grémion, S., V. Pinel, T. Shreve, F. Beauducel, R. Putra, A. Solikhin, A. B. Santoso, and H. Humaida (2023). "Tracking the evolution of the summit lava dome of Merapi volcano between 2018 and 2019 using DEMs derived from TanDEM-X and Pléiades data". *Journal of Volcanology and Geothermal Research* 433, page 107732. ISSN: 0377-0273. DOI: 10.1016/j.jvolgeores.2022.107732.

Hamiel, Y. and G. Baer (2016). "Crustal deformation associated with the 2011 eruption of the Nabro volcano, Eritrea". *Tectonophysics* 691, pages 257–262. ISSN: 0040-1951. DOI: 10.1016/j.tecto.2016.10.013.

Hamling, I. J. (2017). "Crater lake controls on volcano stability: Insights from White Island, New Zealand". *Geophysical Research Letters* 44(22). ISSN: 1944-8007. DOI: 10.1002/2017gl075572.

– (2020). "InSAR observations over the Taupō Volcanic Zone's cone volcanoes: insights and challenges from the New Zealand volcano supersite". *New Zealand Journal of Geology and Geophysics*, pages 1–11. ISSN: 1175-8791. DOI: 10.1080/00288306.2020.1721545.

Hamlyn, J. E., D. Keir, T. J. Wright, J. W. Neuberg, B. Goitom, J. O. S. Hammond, C. Pagli, C. Oppenheimer, J.-M. Kendall, and R. Grandin (2014). "Seismicity and subsidence following the 2011 Nabro eruption, Eritrea: Insights into the plumbing system of an off-rift volcano". *Journal of Geophysical Research: Solid Earth* 119(11), pages 8267–8282. ISSN: 2169-9356. DOI: 10.1002/2014jb011395.

Henderson, S. T., F. Delgado, J. Elliott, M. E. Pritchard, and P. R. Lundgren (2017). "Decelerating uplift at Lazufre volcanic center, Central Andes, from A.D. 2010 to 2016, and implications for geodetic models". *Geosphere* 13(5), pages 1489–1505. ISSN: 1553-040X. DOI: 10.1130/ges01441.1.

Himematsu, Y., F. Sigmundsson, and M. Furuya (2019). "Icecap and subglacial crustal deformation inferred from SAR pixel tracking: The 2014 dike intrusion episode in the Bárðarbunga Volcanic System, Iceland". *Journal of Geophysical Research: Solid Earth* 124(9), pages 9940–9955. ISSN: 2169-9356. DOI: 10.1029/2019jb017652.

Hooper, A., D. Bekaert, K. Spaans, and M. Arıkan (2012). "Recent advances in SAR interferometry time series analysis for measuring crustal deformation". *Tectonophysics* 514–517, pages 1–13. ISSN: 0040-1951. DOI: 10.1016/j.tecto.2011.10.013.

Hunt, J. E., D. R. Tappin, S. F. L. Watt, S. Susilohadi, A. Novellino, S. K. Ebmeier, M. Cassidy, S. L. Engwell, S. T. Grilli, M. Hanif, W. S. Priyanto, M. A. Clare, M. Abdurrachman, and U. Udrekh (2021). "Submarine landslide megablocks show half of Anak Krakatau island failed on December 22nd, 2018". *Nature Communications* 12(1). ISSN: 2041-1723. DOI: 10.1038/s41467-021-22610-5.

James, M. R., B. Carr, F. D'Arcy, A. Diefenbach, H. Dietterich, A. Fornaciai, E. Lev, E. Liu, D. Pieri, M. Rodgers, B. Smets, A. Terada, F. Von Aulock, T. Walter, K. Wood, and E. Zorn (2020). "Volcanological applications of unoccupied aircraft systems (UAS): Developments, strategies, and future challenges". *Volcanica* 3(1), pages 67–114. ISSN: 2610-3540. DOI: 10.30909/vol.03.01.67114.

Jay, J. A., F. J. Delgado, J. L. Torres, M. E. Pritchard, O. Macedo, and V. Aguilar (2015). "Deformation and seismicity near Sabancaya volcano, southern Peru, from 2002 to 2015". *Geophysical Research Letters* 42(8), pages 2780–2788. ISSN: 1944-8007. DOI: 10.1002/2015gl063589.

Jolivet, R., P. S. Agram, N. Y. Lin, M. Simons, M.-P. Doin, G. Peltzer, and Z. Li (2014). "Improving InSAR geodesy using global atmospheric models". *Journal of Geophysical Research: Solid Earth* 119(3), pages 2324–2341. ISSN: 2169-9356. DOI: 10.1002/2013jb010588.

Kolzenburg, S., J. Jaenicke, U. Münzer, and D. B. Dingwell (2018). "The effect of inflation on the morphology-derived rheological parameters of lava flows and its implications for interpreting remote sensing data—A case study on the 2014/2015 eruption at Holuhraun, Iceland". *Journal of Volcanology and Geothermal Research* 357, pages 200–212. ISSN: 0377-0273. DOI: 10.1016/j.jvolgeores.2018.04.024.

Kolzenburg, S., M. Favalli, A. Fornaciai, I. Isola, A. J. L. Harris, L. Nannipieri, and D. Giordano (2016). "Rapid updating and improvement of airborne LIDAR DEMs through ground-based SfM 3-D modeling of volcanic features". *IEEE Transactions on Geoscience and Remote Sensing* 54(11), pages 6687–6699. ISSN: 1558-0644. DOI: 10.1109/tgrs.2016.2587798.

Korevaar, A. (2020). "InSAR as a volcanic monitoring tool for Saba and St. Eustatius: A comparison of ALOS-2, Sentinel-1 and PAZ data". Master's thesis. Delft University of Technology.

Koulakov, I., P. Plechov, R. Mania, T. R. Walter, S. Z. Smirnov, I. Abkadyrov, A. Jakovlev, V. Davydova, S. Senyukov, N. Bushenkova, A. Novgorodova, T. Stupina, and S. Y. Droznina (2021). "Anatomy of the Bezymianny volcano merely before an explosive eruption on 20.12.2017". *Scientific Reports* 11(1). ISSN: 2045-2322. DOI: 10.1038/s41598-021-81498-9.

Kubanek, J., M. P. Poland, and J. Biggs (2021). "Applications of bistatic radar to volcano topography—A review of ten years of TanDEM-X". *IEEE Journal of Selected Topics in Applied Earth Observations and Remote Sensing* 14, pages 3282–3302. ISSN: 2151-1535. DOI: 10.1109/jstars.2021.3055653.

Kubanek, J., J. A. Richardson, S. J. Charbonnier, and L. J. Connor (2015a). "Lava flow mapping and volume calculations for the 2012–2013 Tolbachik, Kamchatka, fissure eruption using bistatic TanDEM-X InSAR". *Bulletin of Volcanology* 77(12). ISSN: 1432-0819. DOI: 10.1007/s00445-015-0989-9.

Kubanek, J., M. Westerhaus, A. Heck, B. Raible, and B. Heck (2018). "TanDEM-X in volcanology: Achievements and perspectives". *Proceedings of the European Conference on Synthetic Aperture Radar, EUSAR*, pages 179–184.

Kubanek, J., M. Westerhaus, and B. Heck (2017). "TanDEM-X time series analysis reveals lava flow volume and effusion rates of the 2012–2013 Tolbachik, Kamchatka fissure eruption". *Journal of Geophysical Research: Solid Earth* 122(10), pages 7754–7774. ISSN: 2169-9356. DOI: 10.1002/2017jb014309.

Kubanek, J., M. Westerhaus, A. Schenk, N. Aisyah, K. S. Brotopuspito, and B. Heck (2015b). "Volumetric change quantification of the 2010 Merapi eruption using TanDEM-X InSAR". *Remote Sensing of Environment* 164, pages 16–25. ISSN: 0034-4257. DOI: 10.1016/j.rse.2015.02.027.

Le Mével, H., L. Córdova, C. Cardona, and K. L. Feigl (2021). "Unrest at the Laguna del Maule volcanic field 2005–2020: renewed acceleration of deformation". *Bulletin of Volcanology* 83(6). ISSN: 1432-0819. DOI: 10.1007/s00445-021-01457-0.

Le Mével, H., K. L. Feigl, L. Córdova, C. DeMets, and P. Lundgren (2015). "Evolution of unrest at Laguna del Maule volcanic field (Chile) from InSAR and GPS measurements, 2003 to 2014". *Geophysical Research Letters* 42(16), pages 6590–6598. ISSN: 1944-8007. DOI: 10.1002/2015gl064665.

Loughlin, S. C., S. Sparks, S. K. Brown, S. F. Jenkins, and C. Vye-Brown (2015). *Global Volcanic Hazards and Risk*. Cambridge University Press. ISBN: 9781316276273. DOI: 10.1017/cbo9781316276273.

Lu, Z. and D. Dzurisin (2014). "InSAR Imaging of Aleutian Volcanoes". *InSAR Imaging of Aleutian Volcanoes*. Springer Berlin Heidelberg, pages 87–345. ISBN: 9783642003486. DOI: 10.1007/978-3-642-00348-6_6.

Lundgren, P. R., M. Bagnardi, and H. Dietterich (2019). "Topographic changes during the 2018 Kīlauea eruption from single-pass airborne InSAR". *Geophysical Research Letters* 46(16), pages 9554–9562. ISSN: 1944-8007. DOI: 10.1029/2019gl083501.

MacQueen, P., F. Delgado, K. Reath, M. E. Pritchard, M. Bagnardi, P. Milillo, P. Lundgren, O. Macedo, V. Aguilar, M. Ortega, R. Anccasi, I. A. Lazarte Zerpa, and R. Miranda (2020). "Volcano–tectonic interactions at Sabancaya Volcano, Peru: Eruptions, magmatic inflation, moderate earthquakes, and fault creep". *Journal of Geophysical Research: Solid Earth* 125(5). ISSN: 2169-9356. DOI: 10.1029/2019jb019281.

Maeno, F., S. Nakada, and T. Kaneko (2016). "Morphological evolution of a new volcanic islet sustained by compound lava flows". *Geology* 44(4), pages 259–262. ISSN: 1943-2682. DOI: 10.1130/g37461.1.

Mania, R., T. R. Walter, M. Belousova, A. Belousov, and S. L. Senyukov (2019). "Deformations and morphology changes associated with the 2016–2017 eruption sequence at Bezymianny Volcano, Kamchatka". *Remote Sensing* 11(11), page 1278. ISSN: 2072-4292. DOI: 10.3390/rs11111278.

Martins, J., A. Hooper, K. Spaans, F. Sigmundsson, and K. Feigl (2011). "Analysis of the Eyjafjallajökull 2010 eruption through TerraSAR-X InSAR time series". *EGU General Assembly*.

Matthews, J., H. Kamata, S. Okuyama, Y. Yusa, and H. Shimizu (2003). "Surface height adjustments in pyroclastic-flow deposits observed at Unzen volcano by JERS-1 SAR interferometry". *Journal of Volcanology and Geothermal Research* 125(3–4), pages 247–270. ISSN: 0377-0273. DOI: 10.1016/s0377-0273(03)00112-4.

McKee, K., C. M. Smith, K. Reath, E. Snee, S. Maher, R. S. Matoza, S. Carn, L. Mastin, K. Anderson, D. Damby, D. C. Roman, A. Degterev, A. Rybin, M. Chibisova, J. D. Assink, R. de Negri Leiva, and A. Perttu (2021a). "Evaluating the state-of-the-art in remote volcanic eruption characterization Part I: Raikoke volcano, Kuril Islands". *Journal of Volcanology and Geothermal Research* 419, page 107354. ISSN: 0377-0273. DOI: 10.1016/j.jvolgeores.2021.107354.

McKee, K., C. M. Smith, K. Reath, E. Snee, S. Maher, R. S. Matoza, S. Carn, D. C. Roman, L. Mastin, K. Anderson, D. Damby, I. Itikarai, K. Mulina, S. Saunders, J. D. Assink, R. de Negri Leiva, and A. Perttu (2021b). "Evaluating the state-of-the-art in remote volcanic eruption characterization Part II: Ulawun volcano, Papua New Guinea". *Journal of Volcanology and Geothermal Research* 420, page 107381. ISSN: 0377-0273. DOI: 10.1016/j.jvolgeores.2021.107381.

Michalczewska, K., S. Hreinsdottir, T. Arnadottir, S. Hjaltadottir, T. Agustsdottir, M. T. Gudmundsson, H. Geirsson, F. Sigmundsson, and G. Gudmundsson (2012). "Inflation and deflation episodes in the Krisuvik volcanic system". *AGU Fall Meeting*, V33A-2843.

Michel, R., J.-P. Avouac, and J. Taboury (1999). "Measuring ground displacements from SAR amplitude images: Application to the Landers Earthquake". *Geophysical Research Letters* 26(7), pages 875–878. ISSN: 1944-8007. DOI: 10.1029/1999gl900138.

Minet, C., K. Goel, I. Aquino, R. Avino, G. Berrino, S. Caliro, G. Chidini, P. De Martino, C. Del Gaudio, C. Ricco, V. Siniscalchi, and S. Borgsrtom (2012). "High resolution monitoring of Campi Flegrei (Naples, Italy) by exploiting TerraSAR-X data: An application of Solifatara Crater". *Fringe 2011*. Volume 697. ESA Special Publication, page 28.

Miyagi, Y. (2017). "Geodetic observations using GNSS, tiltmeter, and DInSAR, at Tokachi-dake Volcano, Japan". *AGU Fall Meeting*, V23A-0464.

Muller, C., J. Biggs, S. K. Ebmeier, P. Mothes, P. B. Palacios, P. Jarrín, M. Edmonds, and M. Ruiz (2018). "Temporal evolution of the magmatic system at Tungurahua Volcano, Ecuador, detected by geodetic observations". *Journal of Volcanology and Geothermal Research* 368, pages 63–72. ISSN: 0377-0273. DOI: 10.1016/j.jvolgeores.2018.11.004.

Nakada, S., A. Zaennudin, M. Yoshimoto, F. Maeno, Y. Suzuki, N. Hokanishi, H. Sasaki, M. Iguchi, T. Ohkura, H. Gunawan, and H. Triastuty (2019). "Growth process of the lava dome/flow complex at Sinabung Volcano during 2013–2016". *Journal of Volcanology and Geothermal Research* 382, pages 120–136. ISSN: 0377-0273. DOI: 10.1016/j.jvolgeores.2017.06.012.

National Academies of Sciences, Engineering & Medicine (2017). *Volcanic eruptions and their repose, unrest, precursors, and timing*. National Academies Press. ISBN: 9780309454124. DOI: 10.17226/24650.

Newhall, C. G. and S. Self (1982). "The volcanic explosivity index (VEI) an estimate of explosive magnitude for historical volcanism". *Journal of Geophysical Research: Oceans* 87(C2), pages 1231–1238. ISSN: 0148-0227. DOI: 10.1029/jc087ic02p01231.

Okajima, Y., K. Yoshikawa, and T. Shibayama (2011). "Recent experiences utilizing TerraSAR-X for the monitoring of natural disasters in different parts of the world". *2011 IEEE International Geoscience and Remote Sensing Symposium*. DOI: 10.1109/igarss.2011.6050181.

Pallister, J., R. Wessels, J. Griswold, W. McCausland, N. Kartadinata, H. Gunawan, A. Budianto, and S. Primulyana (2019). "Monitoring, forecasting collapse events, and mapping pyroclastic deposits at Sinabung volcano with satellite imagery". *Journal of Volcanology and Geothermal Research* 382, pages 149–163. ISSN: 0377-0273. DOI: 10.1016/j.jvolgeores.2018.05.012.

Pallister, J. S., D. J. Schneider, J. P. Griswold, R. H. Keeler, W. C. Burton, C. Noyles, C. G. Newhall, and A. Ratdomopurbo (2013). "Merapi 2010 eruption—Chronology and extrusion rates monitored with satellite radar and used in eruption forecasting". *Journal of Volcanology and Geothermal Research* 261, pages 144–152. ISSN: 0377-0273. DOI: 10.1016/j.jvolgeores.2012.07.012.

Papageorgiou, E., M. Foumelis, E. Trasatti, G. Ventura, D. Raucoules, and A. Mouratidis (2019). "Multi-sensor SAR geodetic imaging and modelling of Santorini Volcano post-unrest response". *Remote Sensing* 11(3), page 259. ISSN: 2072-4292. DOI: 10.3390/rs11030259.

Park, S.-J., S. Lee, and C.-W. Lee (2019). "Baekdu volcano lake "Chun-ji" ice dynamic monitoring using TerraSAR-X satellite imagery". *Korean Journal of Remote Sensing* 35(2), pages 327–336.

Parker, A. L., J. Biggs, R. J. Walters, S. K. Ebmeier, T. J. Wright, N. A. Teanby, and Z. Lu (2015). "Systematic assessment of atmospheric uncertainties for InSAR data at volcanic arcs using large-scale atmospheric models: Application to the Cascade volcanoes, United States". *Remote Sensing of Environment* 170, pages 102–114. ISSN: 0034-4257. DOI: 10.1016/j.rse.2015.09.003.

Parks, M. M., J. Biggs, P. England, T. A. Mather, P. Nomikou, K. Palamartchouk, X. Papanikolaou, D. Paradissis, B. Parsons, D. M. Pyle, C. Raptakis, and V. Zacharis (2012). "Evolution of Santorini Volcano dominated by episodic and rapid fluxes of melt from depth". *Nature Geoscience* 5(10), pages 749–754. ISSN: 1752-0908. DOI: 10.1038/ngeo1562.

Pinel, V., M. Poland, and A. Hooper (2014). "Volcanology: Lessons learned from Synthetic Aperture Radar imagery". *Journal of Volcanology and Geothermal Research* 289, pages 81–113. ISSN: 0377-0273. DOI: 10.1016/j.jvolgeores.2014.10.010.

Plank, S., F. Marchese, N. Genzano, M. Nolde, and S. Martinis (2020). "The short life of the volcanic island New Late'iki (Tonga) analyzed by multi-sensor remote sensing data". *Scientific Reports* 10(1). ISSN: 2045-2322. DOI: 10.1038/s41598-020-79261-7.

Plank, S., A. V. Shevchenko, P. d'Angelo, V. Gstaiger, P. J. González, S. Cesca, S. Martinis, and T. R. Walter (2023). "Combining thermal, tri-stereo optical and bi-static InSAR satellite imagery for lava volume estimates: the 2021 Cumbre Vieja eruption, La Palma". *Scientific Reports* 13(1). ISSN: 2045-2322. DOI: 10.1038/s41598-023-29061-6.

Plank, S., T. R. Walter, S. Martinis, and S. Cesca (2019). "Growth and collapse of a littoral lava dome during the 2018/19 eruption of Kadovar Volcano, Papua New Guinea, analyzed by multi-sensor satellite imagery". *Journal of Volcanology and Geothermal Research* 388, page 106704. ISSN: 0377-0273. DOI: 10.1016/j.jvolgeores.2019.106704.

Poland, M. P. (2014). "Time-averaged discharge rate of subaerial lava at Kīlauea Volcano, Hawai'i, measured from TanDEM-X interferometry: Implications for magma supply and storage during 2011–2013". *Journal of Geophysical Research: Solid Earth* 119(7), pages 5464–5481. ISSN: 2169-9356. DOI: 10.1002/2014jb011132.

Poland, M. P., T. Lopez, R. Wright, and M. J. Pavolonis (2020). "Forecasting, detecting, and tracking volcanic eruptions from space". *Remote Sensing in Earth Systems Sciences* 3(1–2), pages 55–94. ISSN: 2520-8209. DOI: 10.1007/s41976-020-00034-x.

Poland, M. P. and H. A. Zebker (2022). "Volcano geodesy using InSAR in 2020: the past and next decades". *Bulletin of Volcanology* 84(3). ISSN: 1432-0819. DOI: 10.1007/s00445-022-01531-1.

Pritchard, M. E., J. Biggs, C. Wauthier, E. Sansosti, D. W. D. Arnold, F. Delgado, S. K. Ebmeier, S. T. Henderson, K. Stephens, C. Cooper, K. Wnuk, F. Amelung, V. Aguilar, P. Mothes, O. Macedo, L. E. Lara, M. P. Poland, and S. Zoffoli (2018). "Towards coordinated regional multi-satellite InSAR volcano observations: results from the Latin America pilot project". *Journal of Applied Volcanology* 7(1). ISSN: 2191-5040. DOI: 10.1186/s13617-018-0074-0.

Pritchard, M. E., M. Poland, K. Reath, B. Andrews, M. Bagnardi, J. Biggs, S. Carn, D. Coppola, S. K. Ebmeier, M. A. Furtney, T. Girona, J. Griswold, T. Lopez, P. Lundgren, S. Ogburn, M. Pavolonis, E. Rumpf, G. Vaughan, C. Wauthier, R. Wessels, R. Wright, K. R. Anderson, M. G. Bato, and A. Roman (2022a). *Optimizing satellite resources for the global assessment and mitigation of volcanic hazards—Suggestions from the USGS Powell Center volcano remote sensing working group: U.S. Geological Survey Scientific Investigations Report 2022–5116*. 69 pages. DOI: 10.3133/sir20225116.

Pritchard, M. E. and S.-H. Yun (2018). "Satellite radar imaging and its application to natural hazards". *Natural Hazards*. Edited by R. Singh and D. Bartlett, pages 95–114.

Pritchard, M. E., S. K. Ebmeier, M. P. Poland, F. Albino, J. Biggs, F. Delgado, E. W. Dualeh, R. Grandin, F. Galetto, I. J. Hamling, Y. Aoki, M. Bemelmans, and E. Sansosti (2022b). "Aiming the firehose of data at the fire: Optimizing international satellite SAR observations for volcano hazards with the CEOS volcano demonstrator project". *AGU Fall Meeting*, G46A-01.

Qu, F., Z. Lu, M. Poland, J. Freymueller, Q. Zhang, and H.-S. Jung (2015). "Post-eruptive inflation of Okmok Volcano, Alaska, from InSAR, 2008–2014". *Remote Sensing* 7(12), pages 16778–16794. ISSN: 2072-4292. DOI: 10.3390/rs71215839.

Reath, K., M. Pritchard, M. Poland, F. Delgado, S. Carn, D. Coppola, B. Andrews, S. K. Ebmeier, E. Rumpf, S. Henderson, S. Baker, P. Lundgren, R. Wright, J. Biggs, T. Lopez, C. Wauthier, S. Moruzzi, A. Alcott, R. Wessels, J. Griswold, S. Ogburn, S. Loughlin, F. Meyer, G. Vaughan, and M. Bagnardi (2019). "Thermal, deformation, and degassing remote sensing time series (CE 2000–2017) at the 47 most active volcanoes in Latin America: Implications for volcanic systems". *Journal of Geophysical Research: Solid Earth* 124(1), pages 195–218. ISSN: 2169-9356. DOI: 10.1029/2018jb016199.

Richter, N., M. Favalli, E. de Zeeuw-van Dalfsen, A. Fornaciai, R. M. da Silva Fernandes, N. M. Pérez, J. Levy, S. S. Victória, and T. R. Walter (2016). "Lava flow hazard at Fogo Volcano, Cabo Verde, before and after the 2014–2015 eruption". *Natural Hazards and Earth System Sciences* 16(8), pages 1925–1951. ISSN: 1684-9981. DOI: 10.5194/nhess-16-1925-2016.

Richter, N., F. Massimetti, T. Hart, O. Cartus, S. Leinss, A. Derrien, E. Zorn, A. Shevchenko, P. Wintersteller, M. Meschede, and T. Walter (2023). "Volcano processes at the remote South Sandwich Islands of Zavodovski and Saunders observed from air and space". DOI: 10.5194/egusphere-egu23-17100.

Richter, N., M. P. Poland, and P. R. Lundgren (2013). "TerraSAR-X interferometry reveals small-scale deformation associated with the summit eruption of Kīlauea Volcano, Hawai'i". *Geophysical Research Letters* 40(7), pages 1279–1283. ISSN: 1944-8007. DOI: 10.1002/grl.50286.

Richter, N., J. T. Salzer, E. de Zeeuw-van Dalfsen, D. Perissin, and T. R. Walter (2018). "Constraints on the geomorphological evolution of the nested summit craters of Láscar volcano from high spatio-temporal resolution TerraSAR-X interferometry". *Bulletin of Volcanology* 80(3). ISSN: 1432-0819. DOI: 10.1007/s00445-018-1195-3.

Riegler, G., S. D. Hennig, and M. Weber (2015). "WorldDEM—a novel global foundation layer". *The International Archives of the Photogrammetry, Remote Sensing and Spatial Information Sciences* XL-3/W2, pages 183–187. ISSN: 2194-9034. DOI: 10.5194/isprsarchives-xl-3-w2-183-2015.

Rosen, P. A., E. M. Gurrola, P. S. Agram, G. F. Sacco, and M. Lavalle (2015). "The InSAR Scientific Computing Environment (ISCE): A Python Framework for Earth Science". *AGU Fall Meeting*, IN11C-1789.

Ruch, J., T. Wang, W. Xu, M. Hensch, and S. Jónsson (2016). "Oblique rift opening revealed by reoccurring magma injection in central Iceland". *Nature Communications* 7(1). ISSN: 2041-1723. DOI: 10.1038/ncomms12352.

Sacco, P., M. G. Daraio, M. L. Battagliere, and A. Coletta (2015). "Mitigation of volcanic risk: The COSMO-SkyMed contribution". *Fringe 2015*. Volume 731. ESA Special Publication, 26.

Salvi, S. (2016). "The GEO geohazard supersites and natural laboratories - GSNL 2.0: improving societal benefits of geohazard science". *EGU General Assembly*.

Salzer, J. T., P. Milillo, N. Varley, D. Perissin, M. Pantaleo, and T. R. Walter (2017). "Evaluating links between deformation, topography and surface temperature at volcanic domes: Results from a multi-sensor study at Volcán de Colima, Mexico". *Earth and Planetary Science Letters* 479, pages 354–365. ISSN: 0012-821X. DOI: 10.1016/j.epsl.2017.09.027.

Salzer, J. T., M. Nikkhoo, T. R. Walter, H. Sudhaus, G. Reyes-Dávila, M. Bretón, and R. Arámbula (2014). "Satellite radar data reveal short-term pre-explosive displacements and a complex conduit system at Volcán de Colima, Mexico". *Frontiers in Earth Science* 2. ISSN: 2296-6463. DOI: 10.3389/feart.2014.00012.

Sango, D., S. Kusano, T. Shibayama, and K. Yoshikawa (2015). "A study for the methodology to monitor Mt. Shinmoe-dake Volcano by combining ALOS-2, RADARSAT-2, and TerraSAR-X satellite data". *35th Asian Conference on Remote Sensing*.

Sansosti, E., M. P. Poland, J. Biggs, M. E. Pritchard, P. Lundgren, S. K. Ebmeier, and S. Zoffoli (2019). "The CEOS volcano demonstrator for Latin America, Southeast Asia, and Africa overview". *ESA Living Planet Symposium*.

Shreve, T. (2020). "Crustal deformation at Ambrym (Vanuatu) imaged with satellite geodesy: Constraints on magma storage, migration, and outgassing". Ph.D. Thesis. Université Paris Cité.

Shreve, T. and F. Delgado (2023). "Trapdoor fault activation: A step toward caldera collapse at Sierra Negra, Galápagos, Ecuador". *Journal of Geophysical Research: Solid Earth* 128(5). ISSN: 2169-9356. DOI: 10.1029/2023jb026437.

Shreve, T., Y. Zhan, H. Le Mével, D. Roman, and Y. Moussallam (2023). "Two distinct magma storage regions at Ambrym Volcano detected by satellite geodesy". *Geophysical Research Letters* 50(15). ISSN: 1944-8007. DOI: 10.1029/2023gl102925.

Sica, F., S. Bretzke, A. Pulella, J.-L. Bueso-Bello, M. Martone, P. Prats-Iraola, M.-J. Gonzalez-Bonilla, M. Schmitt, and P. Rizzoli (2021). "InSAR decorrelation at X-band from the joint TanDEM-X/PAZ constellation". *IEEE Geoscience and Remote Sensing Letters* 18(12), pages 2107–2111. ISSN: 1558-0571. DOI: 10.1109/lgrs.2020.3014809.

Sigmundsson, F., A. Hooper, S. Hreinsdóttir, K. S. Vogfjörd, B. G. Ófeigsson, E. R. Heimisson, S. Dumont, M. Parks, K. Spaans, G. B. Gudmundsson, V. Drouin, T. Árnadóttir, K. Jónsdóttir, M. T. Gudmundsson, T. Högnadóttir, H. M. Fridriksdóttir, M. Hensch, P. Einarsson, E. Magnússon, S. Samsonov, B. Brandsdóttir, R. S. White, T. Ágústsdóttir, T. Greenfield, R. G. Green, Á. R. Hjartardóttir, R. Pedersen, R. A. Bennett, H. Geirsson, P. C. La Femina, H. Björnsson, F. Pálsson, E. Sturkell, C. J. Bean, M. Möllhoff, A. K. Braiden, and E. P. S. Eibl (2014). "Segmented lateral dyke growth in a rifting event at Bárðarbunga volcanic system, Iceland". *Nature* 517(7533), pages 191–195. ISSN: 1476-4687. DOI: 10.1038/nature14111.

Sigmundsson, F., S. Hreinsdóttir, A. Hooper, T. Árnadóttir, R. Pedersen, M. J. Roberts, N. Óskarsson, A. Auriac, J. Decriem, P. Einarsson, H. Geirsson, M. Hensch, B. G. Ófeigsson, E. Sturkell, H. Sveinbjörnsson, and K. L. Feigl (2010). "Intrusion triggering of the 2010 Eyjafjallajökull explosive eruption". *Nature* 468(7322), pages 426–430. ISSN: 1476-4687. DOI: 10.1038/nature09558.

Smittarello, D., R. Grandin, M. Jaspard, D. Derauw, N. d'Oreye, T. Shreve, M. Debret, N. Theys, and H. Brenot (2023). "Nyiragongo crater collapses measured by multi-sensor SAR amplitude time series". *Journal of Geophysical Research: Solid Earth* 128(10). ISSN: 2169-9356. DOI: 10.1029/2023jb026683.

Stephens, K. J., C. Wauthier, R. C. Bussard, M. Higgins, and P. C. LaFemina (2020). "Assessment of mitigation strategies for tropospheric phase contributions to InSAR time-series datasets over two Nicaraguan volcanoes". *Remote Sensing* 12(5), page 782. ISSN: 2072-4292. DOI: 10.3390/rs12050782.

Valade, S., D. Coppola, R. Campion, A. Ley, T. Boulesteix, N. Taquet, D. Legrand, M. Laiolo, T. R. Walter, and S. De la Cruz-Reyna (2023). "Lava dome cycles reveal rise and fall of magma column at Popocatépetl volcano". *Nature Communications* 14(1). ISSN: 2041-1723. DOI: 10.1038/s41467-023-38386-9.

Valade, S., A. Ley, F. Massimetti, O. D'Hondt, M. Laiolo, D. Coppola, D. Loibl, O. Hellwich, and T. R. Walter (2019). "Towards global volcano monitoring using multisensor Sentinel missions and artificial intelligence: The MOUNTS monitoring system". *Remote Sensing* 11(13), page 1528. ISSN: 2072-4292. DOI: 10.3390/rs11131528.

Vasco, D. W., J. Rutqvist, A. Ferretti, A. Rucci, F. Bellotti, P. Dobson, C. Oldenburg, J. Garcia, M. Walters, and C. Hartline (2013). "Monitoring deformation at the Geysers Geothermal Field, California using C-band and X-band interferometric synthetic aperture radar". *Geophysical Research Letters* 40(11), pages 2567–2572. ISSN: 1944-8007. DOI: 10.1002/grl.50314.

Wadge, G., P. Cole, A. Stinton, J.-C. Komorowski, R. Stewart, A. Toombs, and Y. Legendre (2011). "Rapid topographic change measured by high-resolution satellite radar at Soufriere Hills Volcano, Montserrat, 2008–2010". *Journal of Volcanology and Geothermal Research* 199(1–2), pages 142–152. ISSN: 0377-0273. DOI: 10.1016/j.jvolgeores.2010.10.011.

Wadge, G., S. Saunders, and I. Itikarai (2012). "Pulsatory andesite lava flow at Bagana Volcano". *Geochemistry, Geophysics, Geosystems* 13(11). ISSN: 1525-2027. DOI: 10.1029/2012gc004336.

Walter, T. R. (2023). "Radar sensing of Merapi Volcano". *Active Volcanoes of the World*. Springer International Publishing, pages 437–456. ISBN: 9783031150401. DOI: 10.1007/978-3-031-15040-1_14.

Walter, T. R., M. Haghshenas Haghighi, F. M. Schneider, D. Coppola, M. Motagh, J. Saul, A. Babeyko, T. Dahm, V. R. Troll, F. Tilmann, S. Heimann, S. Valade, R. Triyono, R. Khomarudin, N. Kartadinata, M. Laiolo, F. Massimetti, and P. Gaebler (2019a). "Complex hazard cascade culminating in the Anak Krakatau sector collapse". *Nature Communications* 10(1). ISSN: 2041-1723. DOI: 10.1038/s41467-019-12284-5.

Walter, T. R., C. E. Harnett, N. Varley, D. V. Bracamontes, J. Salzer, E. U. Zorn, M. Bretón, R. Arámbula, and M. E. Thomas (2019b). "Imaging the 2013 explosive crater excavation and new dome formation at Volcán de Colima with TerraSAR-X, time-lapse cameras and modelling". *Journal of Volcanology and Geothermal Research* 369, pages 224–237. ISSN: 0377-0273. DOI: 10.1016/j.jvolgeores.2018.11.016.

Walter, T. R., E. U. Zorn, C. E. Harnett, A. V. Shevchenko, A. Belousov, M. Belousova, and M. S. Vassileva (2022). "Influence of conduit and topography complexity on spine extrusion at Shiveluch volcano, Kamchatka". *Communications Earth & Environment* 3(1). ISSN: 2662-4435. DOI: 10.1038/s43247-022-00491-w.

Wang, J., Z. Lu, and P. Gregg (2021). "Deformation mapping and source modeling of the Makushin volcano during 2011 to 2021". *AGU Fall Meeting Abstracts*, G25A-0339.

Wang, T., K. DeGrandpre, Z. Lu, and J. T. Freymueller (2018). "Complex surface deformation of Akutan volcano, Alaska revealed from InSAR time series". *International Journal of Applied Earth Observation and Geoinformation* 64, pages 171–180. ISSN: 1569-8432. DOI: 10.1016/j.jag.2017.09.001.

Wang, T., M. P. Poland, and Z. Lu (2015). "Dome growth at Mount Cleveland, Aleutian Arc, quantified by time series TerraSAR-X imagery". *Geophysical Research Letters* 42(24). ISSN: 1944-8007. DOI: 10.1002/2015gl066784.

Waythomas, C. F., K. Angeli, and R. L. Wessels (2020). "Evolution of the submarine–subaerial edifice of Bogoslof volcano, Alaska, during its 2016–2017 eruption based on analysis of satellite imagery". *Bulletin of Volcanology* 82(2). ISSN: 1432-0819. DOI: 10.1007/s00445-020-1363-0.

Werner, C., U. Wegmüller, T. Strozzi, and A. Wiesmann (2000). "GAMMA SAR and interferometric processing software". *ERS - ENVISAT Symposium*.

Wessel, B. (2018). *TanDEM-X ground segment—DEM products specification document*.

Whitehead, M. G. and M. S. Bebbington (2021). "Method selection in short-term eruption forecasting". *Journal of Volcanology and Geothermal Research* 419, page 107386. ISSN: 0377-0273. DOI: 10.1016/j.jvolgeores.2021.107386.

Wicks, C. W., D. Dzurisin, J. B. Lowenstern, and J. Svarc (2020). "Magma intrusion and volatile ascent beneath Norris geyser basin, Yellowstone National Park". *Journal of Geophysical Research: Solid Earth* 125(2). ISSN: 2169-9356. DOI: 10.1029/2019jb018208.

Wright, T. J., B. E. Parsons, and Z. Lu (2004). "Toward mapping surface deformation in three dimensions using InSAR". *Geophysical Research Letters* 31(1). ISSN: 1944-8007. DOI: 10.1029/2003gl018827.

Xu, W., J. Ruch, and S. Jónsson (2015). "Birth of two volcanic islands in the southern Red Sea". *Nature Communications* 6(1). ISSN: 2041-1723. DOI: 10.1038/ncomms8104.

Xu, W., L. Xie, R. Bürgmann, X. Liu, and J. Wang (2023). "The 2022 eruption of Wolf Volcano, Galápagos: The role of caldera ring-faults during magma transfer from InSAR deformation data". *Geophysical Research Letters* 50(14). ISSN: 1944-8007. DOI: 10.1029/2023gl103704.

Yunjun, Z., H. Fattahi, and F. Amelung (2019). "Small baseline InSAR time series analysis: Unwrapping error correction and noise reduction". *Computers & Geosciences* 133, page 104331. ISSN: 0098-3004. DOI: 10.1016/j.cageo.2019.104331.

Zebker, H. A., P. Rosen, S. Hensley, and P. J. Mouginis-Mark (1996). "Analysis of active lava flows on Kilauea volcano, Hawaii, using SIR-C radar correlation measurements". *Geology* 24(6), page 495. ISSN: 0091-7613. DOI: 10.1130/0091-7613(1996)024<0495:aoalfo>2.3.co;2.

Zink, M., A. Moreira, I. Hajnsek, P. Rizzoli, M. Bachmann, R. Kahle, T. Fritz, M. Huber, G. Krieger, M. Lachaise, M. Martone, E. Maurer, and B. Wessel (2021). "TanDEM-X: 10 years of formation flying bistatic SAR interferometry". *IEEE Journal of Selected Topics in Applied Earth Observations and Remote Sensing* 14, pages 3546–3565. ISSN: 2151-1535. DOI: 10.1109/jstars.2021.3062286.